Physics – Uspekhi **68** (11) 1131 – 1150 (2025)

REVIEWS OF TOPICAL PROBLEMS

PACS numbers: **05.45. – a**, 92.10.hb

60th ANNIVERSARY OF L.D. LANDAU INSTITUTE FOR THEORETICAL PHYSICS, RAS

Nonlinear generation of currents by waves on liquid surface

S.S. Vergeles, A.A. Levchenko, V.M. Parfenyev

DOI: https://doi.org/10.3367/UFNe.2025.08.039992

Contents

Abstract. Attenuation of surface waves due to viscous dissipation is accompanied by the excitation of slow vortex currents due to the conservation of total momentum. We present a theoretical model for small-amplitude waves that explains experiments on vortex flow generation by crossing waves. Special attention is paid to the effect of surface contaminants, which is accounted for within the framework of a model of a thin elastic liquid film, leading to enhanced wave dissipation and intensified vortex currents. As the amplitude of the currents increases, their interaction with the waves must be considered. A theoretical framework is proposed to describe this interaction, demonstrating its applicability to classical problems: Guyon waves, the propagation of short waves against a current, and Langmuir circulation. Finally, experimental data on the turbulent regime of flow generation, which occurs at sufficiently large wave amplitudes, are described, and open questions in this field are outlined.

Keywords: waves on liquid surface, surface film, vortex flow, mass current, Stokes drift, virtual wave stress, vortex force, wave scattering and refraction

S.S. Vergeles [1, 2, a], **A.A. Levchenko** [3, b], **V.M. Parfenyev** [1, 2, c]

[1] Landau Institute for Theoretical Physics, Russian Academy of Sciences, prosp. Akademika Semenova 1A, 142432 Chernogolovka, Moscow region, Russian Federation

[2] HSE University, ul. Myasnitskaya 20, 101000 Moscow, Russian Federation

[3] Osipyan Institute of Solid State Physics, Russian Academy of Sciences, ul. Akademika Osipyana 2, 142432 Chernogolovka, Moscow region, Russian Federation

E-mail: [a] ssver@itp.ac.ru, [b] levch@issp.ac.ru, [c] parfenius@gmail.com

Received 30 March 2025, revised 3 August 2025

Uspekhi Fizicheskikh Nauk **195** (11) 1199 – 1220 (2025)

Translated by the authors

1. Introduction

A mass transfer in a horizontal direction beneath a surface of a liquid under excited wave motion has long been a subject of both theoretical research and practical interest. The first attempt to explain this phenomenon was the classic study by G.G. Stokes [1]. This work examined mass transfer in a traveling wave in an ideal fluid, so that the flow remains potential everywhere. It was shown that the motion of Lagrangian particles, averaged over the wave oscillation period, is characterized by a drift velocity that is quadratic in the wave amplitude. Later, M. Longuet-Higgins discovered that fluid viscosity disrupts the potential approximation not only in the linear order of the wave amplitude within the viscous sublayer near the surface but also in the quadratic order, significantly altering the time-averaged mass transport velocity [2].

The influence of fluid viscosity on mass transport can be explained as follows. A traveling surface wave possesses momentum directed along its direction of propagation. The surface density of this momentum is proportional to the square of the wave amplitude. It coincides with the vertically integrated mass flux in the form of Stokes drift. Viscous

dissipation leads to a weakening of the wave amplitude as it propagates. The momentum associated with the wave motion also decreases. However, due to the law of conservation of momentum, the missing momentum is transferred to the fluid. This transfer occurs through the action of a virtual force applied in a thin surface layer that includes wave crests and troughs, as well as the viscous sublayer. This force — the virtual wave shear stress — is proportional to the fluid viscosity and the square of the wave amplitude [3, 4]. The action of this force leads to the generation of a slow shear flow, which then propagates into the bulk of the fluid through viscous diffusion. If the generated current is weak, such that it is not turbulent, then its amplitude in the steady state does not depend on the fluid viscosity, although the viscosity serves as the origin for the current. Subsequent work on this topic has been aimed at reformulating the problem in a Lagrangian description and adapting the main result for oceanography — investigating the nonstationary case and the influence of Coriolis forces [5–10]. From a methodological point of view, [11] is also of interest, as it compares different mathematical approaches to describing the phenomenon.

In the 2010s, interest in the generation of flows by waves arose again, but in a more complex formulation: how would the mass transport be arranged if two crossing waves [12–16], a geometrically more complex wave pattern [17–20], or chaotic wave motion [21–25] was excited on the surface of the liquid? The theoretical analysis for a liquid with a clean free surface, on which two standing orthogonal waves are excited, showed that the lattice of near-surface vortices with the period determined by the wavelength was formed in the stationary/steady-state regime [12]. In the vortices, the vertical velocity component is zero. Therefore, they are completely characterized by the vertical component of vorticity, the distribution of which in the space forms a 'chessboard.' The theory developed in [12] explained many qualitative peculiarities of the excited flow, in particular, its spatial structure and the proportionality of the flow amplitude to the product of amplitudes of the waves and the sine of the phase difference between them. However, numerical agreement was not achieved: in the experiment, the flow amplitude turned out to be an order of magnitude higher than the theoretical predictions.

The reason was that the water surface under real conditions is always covered by a thin film, which leads to a change in the boundary conditions on the liquid surface. In particular, this change causes a sharp increase in the wave damping rate, while barely altering its dispersion relation. The role of the surface film in wave dynamics has been investigated in a number of theoretical studies (see the work by V.G. Levich [26–28] and other authors [29, 30]), as well as in experimental work [31, 32]. Among other things, the increased dissipation of waves on the water surface due to the presence of a film prevents the experimental observation of the inverse cascade in weak turbulence of gravity waves [33]. In one of the early studies [34] on this topic, it was noted that the wave damping rate can change over time. This means that the surface film is a result of the adsorption process of surfactant molecules from the flow-bounding surfaces or from the air, which are captured by the water due to its high dielectric constant.

The influence of a surface film on wave-induced current generation was investigated in detail only recently in [35–37]. The initial idea was that, since the presence of a film increases the wave attenuation, the virtual wave shear stress should increase correspondingly. Initially, the analysis was carried out for the case of an almost incompressible film [35], but a more thorough analysis of experimental data later showed that the horizontal component of the velocity in a wave on a liquid surface does not vanish [37]. This observation indicated that the water surface is covered by a compressible film.

The properties of the film are unknown a priori since the process of its formation is uncontrolled. In a general case, its rheological properties can be described by four coefficients, assuming a weak degree of film deformation: elastic dilation modulus, second viscosity (determining the film's dissipative response to dilation/compression), elastic shear modulus, and first (shear) viscosity [38]. In [36, 37], we assumed that dissipation due to the film's internal viscosity is small compared to the viscous dissipation in the bulk fluid, and, on this basis, we disregarded both of the film's viscosities. Furthermore, we assumed the film to be liquid, meaning it offers no resistance to shear deformations. The criterion for this approximation is the experimental fact of the excitation of vortex flows [37]. A counterexample is the experimental study [39], where a specially prepared film possessed shear elasticity, and therefore horizontal vortex flows were suppressed. Finally, we considered that the film is formed by insoluble molecules, so the mass of the film (the amount of substance in it) is conserved. As a result, the film's properties in our model were described by only one parameter — the elastic dilation modulus [36]. Although this model is simplified and does not cover all possible cases, it was shown in [37] to describe the experimental results sufficiently well.

When the amplitude of orthogonal surface waves increases, along with the 'chessboard' of vortices, a large-scale flow with the size of the entire experimental cell is developed in the system at long times [13, 37]. In the mentioned studies, the waves were excited by oscillating plungers installed along the walls of a rectangular basin. Since the plungers were 2–3 cm short of the edges of the basin, they also excited low-amplitude oblique waves propagating at a small angle to the basin walls due to the edge effects [17]. The nonlinear interaction between waves propagating strictly parallel to the walls of the basin and the oblique waves results in the generation of a large-scale flow with an amplitude inversely proportional to the sine of half the angle between the wave propagation directions [40]. Hence, the small amplitude of the oblique waves is compensated by the smallness of the angle. The proposed mechanism was specifically investigated in experimental study [41].

The phenomenon we are discussing — the generation of vortex flows by waves in an initially quiescent fluid — is representative of a general class of flows that arise at the second order in the amplitude of some oscillatory forcing due to the existence of a viscous boundary layer [42]. Other examples of this class are:

- acoustic flows excited in a low-viscosity liquid by acoustic waves [43, 44] (see also [45, § 80]),
- vortical geostrophic flows, driven by inertial waves [46, 47],
- flows generated by surface waves in a viscous boundary layer near the bottom [2],
- flows caused by a solid body rapidly oscillating in a liquid [48, 49].
- flows associated with bending vibrations of freely suspended films [50–52].

In all cases, the slow flow results from the averaging of the Reynolds tensor in a viscous boundary layer near a solid

boundary or a free surface. A characteristic property of steady-state acoustic flows and viscous flows excited in a viscous boundary layer near a solid wall or a free surface without a film is the independence of their amplitude from viscosity. The case of a contaminated surface covered with a film under consideration violates this rule: the intensity of steady-state slow flows is inversely proportional to the root of the viscosity, provided the elastic compression modulus of the film is sufficiently large.

Increasing the amplitude of surface waves allows reaching a turbulent regime in surface currents. For example, in [21–25], wave motion was excited via the Faraday instability, while in [53], waves in a square cell were excited by two plungers located on adjacent sides. Note also that, under certain conditions, nonlinear four-wave interaction in such a system can lead to the excitation of waves with other frequencies [54]. It is noteworthy that the statistical properties of slow near-surface flows in such systems show a number of features characteristic of two-dimensional turbulence [55], and this holds true even for experiments in deep water. In particular, the energy spectrum of the surface flow is $\propto k^{-5/3}$, the third-order velocity structure function depends linearly on the distance between points and has the sign corresponding to an inverse energy cascade, and, with a decrease in the cell size, the formation of a large-scale coherent vortex is observed [22]. Recent experiments [24, 25], which were aimed at studying the penetration of surface flows into the interior, confirm that the energy of the horizontal flows decreases rapidly with depth and is localized in the vertical direction on a scale of about half the wavelength. At the same time, the divergence of the horizontal velocity is not zero, i.e., the surface interacts with the bulk due to the formation of vertical jets. Currently, there is no consistent theoretical picture explaining all these results.

This theory must also account for the fact that, as the amplitude of the vortex flow increases, its interaction with the fast surface waves can no longer be neglected. The criterion for the relative insignificance of this interaction is the smallness of the vorticity amplitude of the vortex flow compared to the wave damping rate. Otherwise, one must consider the bulk force [56], known as the vortex force [57], which acts from the waves on the vortex flow and arises due to the weak distortion of the wave field by the slow current. On the other hand, the surface waves themselves are refracted and scattered by the spatially inhomogeneous vortex flow. Currently, the role played by the wave-current interaction in experiments [13, 17, 21–25, 53, 54] remains unexplored. Our estimates, provided in this review, show that this interaction, in order of magnitude, is comparable to, or even exceeds, the effect of virtual surface stress. Thus, when constructing a statistical theory of inverse cascade phenomena in the surface layer in the presence of surface waves, it appears impossible to avoid accounting for the interaction between these two subsystems.

To provide a theoretical foundation for future research on this issue, we present an analytical framework developed in recent paper [58]. This framework allows a general description of the mutual influence between waves and the surface current in the limit where the vortex flow can be considered slow, i.e., its rate of change and spatial gradient are small compared to the wave frequency. It is important to emphasize that the framework does not employ any additional simplifications. It adopts a physically justified mathematical picture: the wave velocity field on the background of the slow current is still described by a potential in the zeroth order of interaction; however, a weak vortical correction, unrelated to changes in the surface shape, is added in the first order. Since the framework is new, we find it necessary to demonstrate the technique of its application to already known classical problems, which were solved using other, less universal mathematical formalisms. First, we apply this framework to describe Guyon waves [59], which are studied in terms of the flow function within the perturbation theory [60]. Second, we show how our scheme is reduced to a wave equation when describing the refraction of wave rays in the short-wave limit [61, 62]. We apply the obtained wave equation to study the problem of wave propagation against an enhancing current [63, 64]. As is known, such a current can stop waves. The obtained wave equation completely describes the behavior of a wave near the stopping point, which is not possible when using previous approaches [64]. Third, we describe the result of applying the framework to the problem of Langmuir instability, which arises against the background of a traveling wave and a co-directed shear flow. Previously, the mechanism of Langmuir instability was explained in terms of the concept of a vortex force [65]. It was shown in [58] that consideration of the wave scattering on the Langmuir circulation expanded the structure of the unstable mode by including the scattered wave. The increment of instability of this mode turns out to be greater than that determined in [65]. As a result, we demonstrate the universality of our theoretical framework through these examples.

Our review is organized as follows. In Section 2, we examine the generation of slow flows in the simplest case of a traveling gravity wave. Then, in Section 3, we generalize the analysis to the case of arbitrary wave motion and take into account possible contamination of the surface because of the formation of a thin film. Section 4 focuses on a description of the interaction between slow flows and surface waves. Finally, in Section 5, we discuss the statistical properties of slow flows in the turbulent regime and list a number of open questions in this regard. In the Conclusions, we briefly formulate the main results and also point out research areas where they may be in demand.

2. Generation of current by progressive wave

In this section, we will consider the generation of slow current by a plane traveling gravity wave. Our goal is to reveal the nature of this phenomenon and relate it to the law of momentum conservation by considering the simplest example. First, we will recall how gravity waves are described in an ideal fluid and how their momentum is determined. Then, we will discuss how the viscous attenuation of surface waves results in the generation of slow currents. At the end of the section, we will turn to a description of the motion of passive particles that are used in experiments to record the velocity field. We will see that the drift of these particles includes an additional contribution, the Stokes drift [1], which is not directly related to the generated slow flow but is associated only with the wave motion. In conclusion, we will briefly discuss the case of nonmonochromatic waves (wave packets) and analyze the nonlinear potential contribution to the slow current that arises in this case.

2.1 Waves in ideal fluid

Let us consider an irrotational gravity wave in an ideal fluid of infinite depth. The velocity field is potential, $\mathbf{u} = \nabla\phi$, and

incompressible,

$$\Delta\phi = 0\,, \tag{1}$$

and the velocity potential ϕ satisfies the Bernoulli equation inside the fluid [66],

$$\partial_t\phi + \frac{|\nabla\phi|^2}{2} + \frac{P}{\rho} = 0\,. \tag{2}$$

Here, ρ is the density of the fluid, and P is the modified pressure, which includes the gravitational term. Further, we assume that the z-axis is directed vertically, opposite to the gravitational acceleration $\mathbf{g}$, the liquid surface is determined by the equation $z = h(t, x, y)$, and at rest it coincides with the plane $z = 0$. Then, the modified pressure is $P = p + \rho g z$, where p is the internal pressure.

The dynamic equation (2) must be supplemented with boundary conditions on the fluid surface. First, there is the kinematic boundary condition, which means that the fluid surface moves with the fluid velocity $\mathbf{u} = \nabla\phi$, i.e.,

$$\partial_t h = u_z - u_\alpha \partial_\alpha h\,. \tag{3}$$

Here and hereafter, Greek indices take the values x and y, and summation over repeated indices is implied. Second, there is the dynamic boundary condition, which means the equality of the pressure on the fluid surface to the atmospheric pressure (assumed to be zero) in the absence of capillary forces,

$$P - \rho g h = 0\,. \tag{4}$$

We emphasize that expressions (1)–(4) together with $|\nabla\phi| \to 0$ as $z \to -\infty$ form a closed system of nonlinear equations describing irrotational flow of an ideal fluid.

Next, we assume that a gravity wave of small steepness, $|\nabla h| \ll 1$, is excited on the fluid surface. In the linear approximation, this refers to a wave characterized by the dispersion relation $\omega^2 = gk$, where $k > 0$ is the wavenumber and ω is the wave frequency. For a wave propagating along the x direction, one finds

$$P^{(1)} = \rho\omega^2 H \exp(kz)\,\frac{\cos(kx - \omega t)}{k}\,, \tag{5}$$

$$\phi^{(1)} = \omega H \exp(kz)\,\frac{\sin(kx - \omega t)}{k}\,, \tag{6}$$

$$h^{(1)} = H\cos(kx - \omega t)\,, \tag{7}$$

where H is the wave amplitude, and the superscript (1) denotes the linear approximation.

As we will see below, the momentum associated with the wave motion is quadratic in the wave amplitude H. Therefore, to calculate it, we need to find the second-order corrections, which are determined by the following system of equations:

$$\nabla^2\phi^{(2)} = 0\,, \quad \partial_t\phi^{(2)} + \frac{P^{(2)}}{\rho} = -\frac{(u^{(1)})^2}{2}\,, \tag{8}$$

$$\partial_t h^{(2)} - u_z^{(2)}\big|_{z=0} = \partial_z u_z^{(1)}\big|_{z=0}\, h^{(1)} - u_x^{(1)}\big|_{z=0}\,\partial_x h^{(1)}\,, \tag{9}$$

$$P^{(2)}\big|_{z=0} - \rho g h^{(2)} = -\partial_z P^{(1)}\big|_{z=0}\, h^{(1)}\,. \tag{10}$$

Using expressions (5)–(7) and performing straightforward calculations, we obtain

$$P^{(2)} = -\rho\omega^2 H^2\,\frac{\exp(2kz)}{2}\,, \quad \phi^{(2)} = 0\,, \tag{11}$$

$$h^{(2)} = kH^2\,\frac{\cos(2kx - 2\omega t)}{2}\,. \tag{12}$$

We are now ready to introduce the physical quantities of interest using the simplest example of the traveling gravity wave in an ideal fluid. The surface density of momentum is defined as $\pi_x = \rho\langle\int_{-\infty}^{h} \mathrm{d}z\, u_x\rangle$ and describes the mass transport through a cross section of the wave. Here and hereafter, the angle brackets denote averaging over rapid wave oscillations. Up to the second order in the wave amplitude, we obtain

$$\pi_x \simeq \rho\left\langle\int_{-\infty}^{h^{(1)}} \mathrm{d}z\, u_x^{(1)}\right\rangle = \frac{\rho\omega H^2}{2}\,. \tag{13}$$

Note that the integral accumulates near the surface in a thin layer that includes wave crests and troughs.

Next, we introduce the momentum flux density tensor $\Pi_{ik} = p\delta_{ik} + \rho u_i u_k$, which is the ith component of the momentum transferring along the kth axis [45]. Accordingly, the surface density π_{xx} of the flux of the x-component of momentum in the direction of the x-axis, associated solely with the wave motion, is

$$\pi_{xx} = \left\langle\int_{-\infty}^{h} \mathrm{d}z\,\Pi_{xx} + \rho g\int_{-\infty}^{0} \mathrm{d}z\, z\right\rangle. \tag{14}$$

The surface density of the momentum flux is also called radiation stress. In (14), the last term is necessary to subtract the contribution associated with gravity for the unperturbed surface. Up to the second order in the wave amplitude, we find

$$\pi_{xx} \simeq \int_{-\infty}^{0} \mathrm{d}z\left\langle\rho\left(u_x^{(1)}\right)^2 + P^{(2)}\right\rangle + \left\langle\int_{-\infty}^{h^{(1)}} \mathrm{d}z\, P^{(1)} - \rho g\int_{0}^{h^{(1)}} \mathrm{d}z\, z\right\rangle = \frac{\rho\omega^2 H^2}{4k}\,. \tag{15}$$

This result corresponds to the transport of the surface momentum density π_x at the group velocity $c_g = \omega/(2k)$, i.e., $\pi_{xx} = c_g\pi_x$ [67]. The generalization of these considerations to the case of gravity-capillary waves is given in [68].

2.2 Conservation of momentum under conditions of attenuation of surface waves

The viscosity of the liquid results in the attenuation, or damping, of surface waves. We will assume that the kinematic viscosity of the fluid ν is small, so that the dimensionless parameter $\gamma = \sqrt{\nu k^2/\omega} \ll 1$. In laboratory experiments, waves are typically excited by periodic forcing at the boundary, and, in the steady state, their amplitude decays in space, $H = H_0\exp(-4\gamma^2 kx)$. It can be shown that, for a weakly viscous fluid, the expressions for the surface density of momentum (13) and its flux (15) remain the same, except now the spatial attenuation of the wave amplitude must be taken into account.

If the influence of the vertical walls is neglected, the horizontal projection of the total momentum of the wave system should be conserved. Therefore, the decrease in the

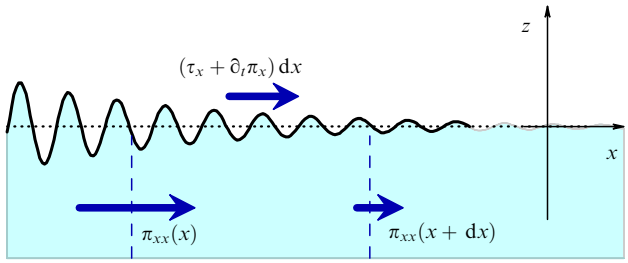

Figure 1. Change in horizontal component of wave motion's momentum generates surface force τ_x (virtual wave stress), which excites slow flow.

momentum of the wave motion associated with the reduction in wave amplitude must be compensated. Physically, this compensation occurs in a thin viscous sublayer near the free surface with a thickness of $\delta \sim \gamma/k$. In this layer, the wave motion ceases to be potential due to the viscosity of the medium. We will examine the structure of the velocity field within the viscous sublayer in detail in the next section, but, for now, for simplicity, we will assume that the thickness of this layer can be disregarded. In this approximation, a shear stress τ_x must be applied to the fluid surface, ensuring the conservation of total momentum:

$$\tau_x = -\partial_t \pi_x - \partial_x \pi_{xx} = 2\rho\nu\omega(kH)^2\,. \tag{16}$$

This expression is illustrated in Fig. 1. The first term on the right-hand side of (16) corresponds to the temporal damping of surface waves [3], which is possible in the general case but absent in our example, and the second term accounts for the spatial attenuation of waves [4]. We emphasize that the imbalance on the right-hand side of (16) leads only to the emergence of a surface force, since, in the bulk, i.e., outside the viscous sublayer, the flow associated with the wave motion remains potential, and therefore the action of nonlinearity cannot generate a slow vortical flow.

The virtual wave stress τ_x transfers momentum from the fast waves to the slow current $\mathbf{V}$, which propagates into the bulk of the fluid because of viscous diffusion. In the initial stage, while the amplitude of the flow $\mathbf{V}$ is small, this process is described by the Navier–Stokes equation

$$\partial_t \mathbf{V} + (\mathbf{V}\nabla)\mathbf{V} = -\frac{\nabla\mathcal{P}}{\rho} + \nu\nabla^2\mathbf{V}\,, \tag{17}$$

$$\operatorname{div}\mathbf{V} = 0\,, \tag{18}$$

where $\mathcal{P}$ is the pressure associated with the slow flow, ensuring the incompressibility condition (18) is satisfied. These equations must be supplemented by boundary conditions on the surface,

$$\rho\nu\partial_z V_x\big|_{z=0} = \tau_x\,, \quad V_z\big|_{z=0} \simeq 0\,, \tag{19}$$

which assume that the slow flow leaves the surface of the liquid flat. Note that, in this approximation, we do not account for the contribution to the Navier–Stokes equation associated with the Craik–Leibovich vortex force [56], which we will discuss in more detail in Section 4.

As an illustration, let us determine the steady slow flow in a fluid layer of thickness d. We assume that this thickness is large compared to the wavelength $\lambda = 2\pi/k$ (the deep-water condition for surface waves), but small compared to the propagation length $l_\nu = 1/(4\gamma^2 k)$. Then, to the leading order in $d/l_\nu \ll 1$, we can solve the equations under the assumption that the force applied to the fluid surface is constant and that the system under consideration is homogeneous along the x-axis. Over a long time, the slow flow will penetrate to the full depth, so we must additionally require that the velocity vanish at the bottom:

$$\mathbf{V}\big|_{z=-d} = 0\,. \tag{20}$$

We will also assume that, in the steady state, there is no net mass transport in the horizontal direction,

$$\int_{-\infty}^{0} V_x(z)\,\mathrm{d}z = 0\,, \tag{21}$$

which is ensured by a corresponding increase in the mean fluid level towards increasing x coordinate. Looking ahead, we note that the correction to this expression due to Stokes drift can be neglected, since $d \gg 1/k$.

Now let us proceed with the calculations. The incompressibility condition (18) leads to $\partial_z V_z = 0$, and, together with the boundary condition (20), this implies that $V_z = 0$. Next, the z-component of equation (17) reduces to $\partial_z\mathcal{P} = 0$, indicating that the pressure is constant in the vertical direction. Considering the x-component of equation (17) together with the boundary conditions (19), (20) and relation (21), we find

$$V_x(z) = \frac{\omega(kH)^2 d}{2}\left(\frac{3z^2}{d^2} + \frac{4z}{d} + 1\right). \tag{22}$$

The obtained answer coincides with the result of [2, Eqn (305)]. Note that, in the limit $\nu \to 0$, the answer remains finite and independent of viscosity, even though the surface force (16) that excites the slow flow is of viscous origin and proportional to it.

2.3 Stokes drift

So far, we have used the Eulerian description of motion, focusing on the structure of the flow velocity field at various points in space. In practice, the velocity of infinitesimal fluid elements, the Lagrangian velocity, is often of greater interest. In laboratory experiments, small particles passively carried by the flow are often added, and their motion is recorded to measure the velocity field. Note that this method imposes a number of constraints on the properties of the particles used. In particular, the particles must accurately follow the fluid motion, must not affect the properties of the flow and the fluid itself, and must not merge in clusters. In the presence of waves, the average Lagrangian velocity differs from the average Eulerian velocity of the flow, even though, at any given moment in time and at any point, these velocities coincide. The difference between these velocities is called the Stokes drift. This phenomenon was first described in the classical study [1], and review [69] can be recommended as modern literature on the subject.

Let us consider the motion of a fluid element along a Lagrangian trajectory when a wave propagates along the surface. The motion of the element is described by the nonlinear equation

$$\frac{\mathrm{d}\mathbf{R}}{\mathrm{d}t} = \mathbf{v}(t, \mathbf{R})\,, \tag{23}$$

where the vector $\mathbf{R}(t)$ describes the position of the Lagrangian particle, and $\mathbf{v}(t,\mathbf{r})$ is the Eulerian flow velocity. In a general case, $\mathbf{v} = \mathbf{u} + \mathbf{V}$, where $\mathbf{u}$ describes the fast wave motion, and $\mathbf{V}$ corresponds to the slow flow.

Suppose that, at the initial moment of time, the Lagrangian particle was located at the point $\mathbf{R}(t_0) = \mathbf{r}_0$. The velocity field in the vicinity of this point can be expanded in a Taylor series

$$v_i(t,\mathbf{r}) = v_i(t,\mathbf{r}_0) + G_{ij}(t,\mathbf{r}_0)(r_j - r_{0j}) + \ldots, \tag{24}$$

where $G_{ij}(t,\mathbf{r}_0) = \partial_j v_i(t,\mathbf{r}_0)$ is the velocity gradient tensor, Latin indices take the values x, y, z, and we sum over repeated indices. Substituting this expansion into equation (23), we find the particle displacement $\delta\mathbf{R} = \delta\mathbf{R}_1 + \delta\mathbf{R}_2$, accurate to the second order in the wave amplitude,

$$\delta\mathbf{R}_1(t) = \int_{t_0}^{t} \mathrm{d}t'\, \mathbf{v}(t',\mathbf{r}_0)\,, \tag{25}$$

$$\delta R_{2i}(t) = \int_{t_0}^{t} \mathrm{d}t'\, G_{ij}(t',\mathbf{r}_0)\, \delta R_{1j}(t')\,, \tag{26}$$

and, to compute $\delta\mathbf{R}_2$, it is sufficient to retain only terms linear in the wave amplitude in $\delta\mathbf{R}_1$ and G_{ij}. Averaging over the rapid wave oscillations, we find the average Lagrangian velocity of the passive particle:

$$V_i^{\mathrm{L}} = V_i + \left\langle G_{ij}(t,\mathbf{r}_0)\, \delta R_{1j}(t) \right\rangle. \tag{27}$$

The last term in expression (27) is called the Stokes drift and is denoted by $\mathbf{U}^{\mathrm{S}}$.

Using expression (6) for the velocity potential of a traveling gravity wave in an ideal fluid, we find

$$\mathbf{U}^{\mathrm{S}} = \left(\omega k H^2 \exp(2kz), 0, 0\right). \tag{28}$$

In the linear approximation, the Lagrangian trajectories in the field of a gravity wave in deep water are circular. Taking into account the second-order terms causes these circles to become open, and the particle slowly drifts in the direction of wave propagation (Fig. 2). The Stokes drift $\mathbf{U}^{\mathrm{S}}$ responds almost instantaneously to changes in the wave amplitude; the corresponding response time can be estimated as the wave oscillation period.

Expression (28) for the Stokes drift remains valid for a weakly viscous fluid outside the viscous sublayer near the surface, since the viscosity has a negligible effect on the potential component of the wave motion velocity. The situation inside the viscous sublayer requires separate consideration, which we will undertake in Section 3. We also note that the mass transport of the fluid through a cross section of the wave can be found by integrating the Stokes drift vertically. The result remains the same:

$$\pi_x \simeq \rho \int_{-\infty}^{0} \mathrm{d}z\, U_x^{\mathrm{S}} = \frac{\rho\omega H^2}{2} \tag{29}$$

(compare with expression (13)). Later, in Section 3.4, we will generalize expressions (28) and (29) to the case of an arbitrary wave field with a narrow spectral width.

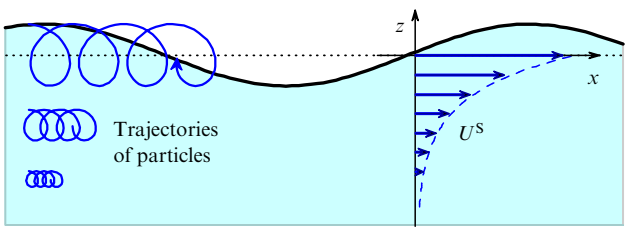

Figure 2. Stokes drift for wave traveling on surface of deep water.

Measuring Stokes drift is a challenging experimental task, because all types of wave-induced Eulerian flows must be eliminated or accounted for. Surprisingly, this problem remains relevant to this day [70]. For example, in recent studies [71, 72], the authors analyzed the trajectories of Lagrangian particles during the passage of a wave packet to measure Stokes drift. The wave field in the form of a wave packet limited in time and space was chosen in order to exclude the excitation of the mean vortical current considered above in Section 2.2. In the case of nonmonochromatic waves, hydrodynamic nonlinearity leads to the emergence of an additional potential contribution to the slow flow, which must be taken into account when processing experimental data. We discuss this contribution in the next section. Its origin is in no way related to the viscosity of the fluid, and it should be distinguished from the slow vortical flow, which is the subject of this review.

2.4 Slow potential flow induced by motion of wave packets

In a weakly nonmonochromatic wave, the surface densities of momentum π_x (13) and its flux π_{xx} (15) vary slowly with coordinate and time even in an ideal fluid. This leads to the emergence of a large-scale slow potential flow component [68], whose velocity we hereafter denote as $\langle\mathbf{u}\rangle$. Although this flow is not the primary subject of interest in this review, we present here the main properties of such slow flows in order to compare them to and distinguish them from the large-scale vortical flows generated by waves in a weakly viscous fluid.

If the spectral width of the wave packet is $\Delta\omega \ll \omega$, then the spatial scale of the slow potential flows is $l \sim c_{\mathrm{g}}/\Delta\omega$ and thus significantly exceeds the wavelength. The velocity of the slow flow is estimated as $\langle u\rangle \sim kH^2\Delta\omega \exp(z/l)$ if the fluid depth d exceeds the characteristic flow scale, $d \gg l$ [72]. Therefore, these flows are weak not only due to the small wave steepness $kH \ll 1$ but also due to the small relative spectral width $\Delta\omega/\omega \ll 1$. It is important to note that the potential nature of these flows implies that the amplitudes of the vertical and horizontal velocities are of the same order of magnitude, $\langle u_z\rangle \sim \langle u_x\rangle$. If the fluid depth still satisfies $kd \gg 1$ but is less than the horizontal size of the wave packet, $l \gg d$, then the velocity estimates are $\langle u_x\rangle \sim \omega H^2/d$ and $\langle u_z\rangle \sim kH^2\Delta\omega(1 + z/d)$ [71]. The horizontal velocity of the flows is directed opposite to the Stokes drift. Near the fluid surface, these flows are weaker by the parameter $\Delta\omega/\omega$ than the Stokes drift, but they penetrate deep into the fluid bulk and, at sufficient depth, can cause Lagrangian particles to drift in the opposite direction compared to particles near the surface. We also note that a detailed mathematical description of wave packet motion is given, for example, in [73], and a discussion of the geometric picture of slow velocity distribution around a spatially localized wave packet can be found in review [74] and monograph [62]. Consideration of the inverse effect of slow flows on a wave is discussed in [75].

For completeness, we mention that the result of the slow potential response to the nonlinear interaction of two waves with a small frequency difference $\Delta\omega$, propagating in

arbitrary directions with wave vectors $\mathbf{k}_1$ and $\mathbf{k}_2$, was considered in [76]. An estimate for the velocity of the slow potential flow in the limiting case $d \gg 1/|\Delta\mathbf{k}|$ is $\langle u\rangle \sim kH^2\Delta\omega$, which coincides with the estimate given above for the velocity of the slow flow induced by plane wave packets. Further in this review, we do not examine the slow potential flow in detail, since its amplitude near the surface is relatively small, and we concentrate on the slow vortical flow and the Stokes drift.

3. Generation of flows by crossing waves on contaminated surface

This section focuses on the analysis of the generation of slow vortex flows when the liquid surface is covered with a thin liquid film. First, we will analyze how the presence of the film changes the velocity field of wave motion and how this velocity field is arranged near the liquid surface inside a thin viscous sublayer. Then, we will trace how the nonlinear term in the Navier–Stokes equation leads to the emergence of a virtual wave stress that excites a slow flow. A theory will be built for an arbitrary form of deviation of the liquid surface from equilibrium. In conclusion, we will briefly review recent experimental studies and discuss their results in the context of the developed theory.

3.1 Equations of motion and boundary conditions

Let us formulate equations that describe the flow of an incompressible fluid, the surface of which is covered with a thin liquid film. In the bulk, the velocity field satisfies the Navier–Stokes equation and the incompressibility condition

$$\partial_t\mathbf{v} + (\mathbf{v}\nabla)\mathbf{v} = -\frac{\nabla P}{\rho} + \nu\nabla^2\mathbf{v}\,, \tag{30}$$

$$\operatorname{div}\mathbf{v} = 0\,. \tag{31}$$

Recall that the Z-axis is directed vertically upwards, and the modified pressure P includes a gravitational term, i.e., $P = p + \rho gz$, where p is the internal pressure. In comparison with the description of the motion of an ideal liquid, we took into account the viscous term that contains second-order spatial derivates of the velocity field and increases the order of the equation. Accordingly, the Navier–Stokes equation requires an additional boundary condition.

Let, as before, the deviation of the surface from the equilibrium position $z = 0$ be described by the function $h(t, x, y)$, which is assumed to be a single-valued function of the coordinates, i.e., we do not consider processes related to the breaking of waves. On the liquid surface $z = h(t, x, y)$, we must require the fulfillment of kinematic and dynamic boundary conditions. The kinematic boundary condition coincides with condition (3) written earlier for a purely potential flow,

$$\partial_t h = v_z - v_\alpha\partial_\alpha h\,. \tag{32}$$

As before, the Greek letters take the values x and y, and the repeating indices are used for summation.

The dynamic boundary condition is significantly modified owing to the consideration of the viscosity of the liquid and the surface film. In fact, this condition means that the total force acting on an arbitrary element of the surface is zero. This requirement is a direct consequence of Newton's second law, where we neglect the term with acceleration, since the film is assumed to be thin and has a negligible mass. We also assume that no forces are applied to the liquid surface from the side of the air. The role of the film is that it changes the coefficient of surface tension $\sigma(n)$ depending on the surface density of the film n. The non-uniformity of the surface tension leads to an additional tangential force, which must be taken into account in the boundary condition [45, § 63]. As a result, by projecting the dynamic boundary condition onto the direction along the normal to the surface $\mathbf{l}$ and onto the tangential plane, we obtain

$$P - 2\rho\nu l_i l_k\partial_i v_k = \rho gh + \sigma K\,, \tag{33}$$

$$\rho\nu\delta^\perp_{ij} l_k(\partial_j v_k + \partial_k v_j) = \sigma'\delta^\perp_{ij}\partial_j n\,. \tag{34}$$

Here, $\delta^\perp_{ij} = \delta_{ij} - l_i l_j$ is the projector onto the tangential plane, K is the average surface curvature equal to the trace of the curvature tensor $K_{ik} = K_{ki} = \delta^\perp_{ij}\partial_j l_k$, and $\sigma' \equiv \partial\sigma/\partial n$. The operator $\delta^\perp_{ij}\partial_j$ does not contain derivatives in the direction perpendicular to the surface. Therefore, when calculating partial derivatives, the concentration field n can be formally considered to be continued from the surface into three-dimensional space in any convenient way. Expression (33) generalizes relation (4) by taking into account the nonzero viscosity of the liquid and additional capillary pressure. As for the balance of forces in the tangential plane (34), this condition is not required for an ideal liquid and is associated with a higher order of the Navier–Stokes equation. We also point out that the unit vector normal to the liquid surface $\mathbf{l}$ can be expressed through the deviation of the surface from equilibrium

$$\mathbf{l}(t, x, y) = \frac{(-\partial_x h, -\partial_y h, 1)}{\sqrt{1 + (\nabla h)^2}}\,. \tag{35}$$

To close the system of equations, it remains for us to describe the dynamics of the surface density of the film, which we shall present here as a function of only two horizontal coordinates, $n = n(t, x, y)$. We shall think of the film as insoluble, which means the conservation of its mass [35]

$$\partial_t n + v_\alpha\partial_\alpha n + n\delta^\perp_{ij}\partial_j v_i = 0\,, \tag{36}$$

where the values of the velocity field and its gradients should be taken on the surface of the liquid. The second term in (36) describes the transfer of the film substance. The third term takes into account the process of the compression/extension of the film; due to the incompressibility of the liquid, the two-dimensional divergence of the velocity is proportional to the normal component of the viscous stress arising in boundary condition (36), $\delta^\perp_{ij}\partial_j v_i = -l_i l_j\partial_i v_j$. As discussed earlier, the model of the film used does not describe the most general case and has limited applicability. Nevertheless, it describes the experiments quite well. The case of a free liquid surface corresponds to the limit $\sigma'(n) \to 0$, and there is no need to describe the surface density of the film in this approximation.

So far, we have discussed the boundary conditions on the surface of the liquid $z = h(t, x, y)$. As for the bottom, it is assumed to be flat and coincident with the plane $z = -d$. All three velocity components must be zero at a solid boundary. In a horizontal plane, the flow is considered unlimited unless otherwise stated. Further, we will often assume the liquid to be infinitely deep.

When describing the vortex flow generated by waves near the surface, it will be convenient to use the vorticity $\boldsymbol{\varpi} = \operatorname{rot}\mathbf{v}$

instead of the velocity $\mathbf{v}$. By taking the curl from the Navier–Stokes equation (30), we find

$$\partial_t \boldsymbol{\varpi} = -(\mathbf{v}\nabla)\boldsymbol{\varpi} + (\boldsymbol{\varpi}\nabla)\mathbf{v} + \nu\nabla^2\boldsymbol{\varpi}\,. \tag{37}$$

The boundary condition for the vorticity component normal to the surface can be obtained by applying the operator $\epsilon_{imq} l_m \partial_q$ (which contains only derivatives along the surface) to both sides of relation (34):

$$l_m l_k \partial_k \varpi_m + (\partial_i v_k + \partial_k v_i)\epsilon_{imq} l_m K_{kq} = 0\,. \tag{38}$$

Here, ϵ_{ijk} is the unit antisymmetric tensor, and $\varpi_i = \epsilon_{ijk}\partial_j v_k$. When deriving Eqn (38), we used the identity $\epsilon_{imq} l_m \partial_q l_i = \epsilon_{imq} l_m K_{qi} = 0$, which can be verified by direct calculations. The surface tension gradient is not included in boundary condition (38), since the surface force arising as a result of the spatial non-uniformity of the surface tension has a potential character. Hereafter, this circumstance significantly simplifies the nonlinear analysis.

3.2 Linear theory of surface waves in presence of film

The linear analysis of surface waves in the system under consideration is well known [26, 28–30]. The dispersion law has two branches: gravity-capillary waves and Marangoni waves. From the viewpoint of film dynamics, gravity-capillary waves are predominantly transverse, while Marangoni waves are longitudinal. Hereafter, we assume that gravity-capillary waves are weakly attenuating. This is ensured if the dimensionless parameter $\gamma = \sqrt{\nu k^2/\omega} \ll 1$, where ω and k are the frequency and wave number of the wave. Marangoni waves attenuate considerably faster; thus, we do not consider them. The velocity field of gravity-capillary waves will be denoted by $\mathbf{u}$. Hereafter, the total velocity field $\mathbf{v}$ will consist of rapid wave motion $\mathbf{u}$ and a slow vortex flow $\mathbf{V}$.

In the linear approximation, all quantities that characterize gravity-capillary waves can be expressed through the deviation of the liquid surface from equilibrium $h(t, x, y) \propto \exp(\mathrm{i}k_\alpha r_\alpha - \mathrm{i}\omega t)$. For deep water $d \gg 1/k$, the velocity field is determined by the expression [36]

$$\begin{aligned} u_\alpha &= \frac{\exp(kz) - D\exp(\varkappa z)}{k\bigl(1-(k/\varkappa)D\bigr)}\,\partial_\alpha\partial_t h\,,\\ u_z &= \frac{\exp(kz) - (k/\varkappa)D\exp(\varkappa z)}{1-(k/\varkappa)D}\,\partial_t h\,, \end{aligned} \tag{39}$$

where $\varkappa = \sqrt{k^2 - \mathrm{i}\omega/\nu}$ (with a positive real part), and all dependence on the film properties is reduced to the factor

$$D = \frac{2\mathrm{i}\gamma - \varepsilon}{\mathrm{i}\gamma(\varkappa^2+k^2)/(\varkappa k) - \varepsilon}\,,\quad \varepsilon = \frac{-n_0\sigma'(n_0)}{\rho\sqrt{\nu\omega^3}/k^2}\,, \tag{40}$$

where n_0 is the equilibrium value of the surface density of the film on a surface at rest, and the parameter $\varepsilon > 0$ can be called the dimensionless elastic compression modulus of the film. This quantity must be positive for the film to be thermodynamically stable [77]. Note that the value of ε not only characterizes the properties of the film but also depends on the parameters of wave motion. At a fixed value of the compression coefficient of the film $-n_0\sigma'(n_0)$, the maximum dimensionless parameter ε is reached in the region of a transition from gravity to capillary waves at $k = \sqrt{5g\rho/\sigma_0}$, where σ_0 is the surface tension at rest.

The expression for velocity field (39) includes two contributions. The first is proportional to $\exp(kz)$ and corresponds to the potential component of the velocity field that penetrates into the liquid to a distance of the order of $1/k$. The second contribution is proportional to $\exp(\varkappa z)$ and results from the viscosity of the liquid. It is localized in a thin viscous sublayer near the surface with the thickness $\delta \sim \gamma/k \ll 1/k$. Outside the viscous sublayer, the second contribution can be disregarded, and the velocity field becomes potential.

In our model, the properties of the film are characterized by one dimensionless parameter $\varepsilon > 0$ and affect the velocity field of the wave through the complex parameter D. The case of a free surface corresponds to $\varepsilon \to 0$ and $D \to 2\varkappa k/(\varkappa^2+k^2)$ and was analyzed in Ref. [12]. The other limiting case, $\varepsilon \to \infty$ and $D \to 1$, describes an almost incompressible film and was described in Ref. [35]. In the intermediate range, the absolute value of the parameter D is of the order of or less than unity; therefore, the factor $kD/\varkappa$ is small at least as $\gamma \ll 1$. This means that the surface film mainly modifies the nonpotential component of the horizontal velocity. Moreover, if $|D| \sim 1$, this nonpotential correction becomes comparable to the potential contribution inside the viscous sublayer. If there is no film on the liquid surface, $|D| \sim \gamma$, and the potential contribution dominates everywhere.

For further calculations, we will need an expression for vorticity in the linear approximation $\boldsymbol{\varpi}^u = \mathrm{rot}\,\mathbf{u}$. It is determined only by the vortex component of the velocity field and, therefore, is localized inside the viscous sublayer. Direct calculation gives

$$\varpi^u_\alpha = \epsilon_{\alpha\beta}\,\frac{(\varkappa^2-k^2)D}{\varkappa k\bigl(1-(k/\varkappa)D\bigr)}\exp(\varkappa z)\partial_\beta\partial_t h\,,\quad \varpi^u_z = 0\,, \tag{41}$$

where $\epsilon_{\alpha\beta}$ is the second-rank unit antisymmetric tensor. The vorticity is directed horizontally in the linear approximation in the wave amplitude and depends significantly on the film properties.

The presence of a film on the liquid surface does not change the dispersion law of surface waves $\omega^2 = gk + \sigma_0 k^3/\rho$ except for a possible change in the equilibrium value σ_0 of the surface tension coefficient. However, the rate of wave attenuation $-\mathrm{Im}\,\omega$ changes significantly [36]:

$$\frac{\mathrm{Im}\,\omega}{\omega} \approx -2\gamma^2 - \frac{\gamma}{2\sqrt{2}}\,\frac{\varepsilon^2}{\varepsilon^2 - \varepsilon\sqrt{2}+1}\,. \tag{42}$$

The second term in expression (42) becomes the leading one if $\varepsilon \gg \sqrt{\gamma}$, and the attenuation of waves reaches its maximum at the finite compressibility of the film $\varepsilon = \sqrt{2}$ (Fig. 3a). Physically, this behavior is related to the proximity of resonance between gravity-capillary waves and Marangoni waves [77–79]. Note that expression (42) does not take into account dissipation associated with friction at the boundaries of the system, which may be important in laboratory experiments, and depends on the size of an experimental setup and the parameters of wave motion (see Ref. [37] and [45, § 25]). Formula (42) corrected for friction at the boundaries can be used to infer the value of the elastic compression modulus of the film ε from experimental measurements of the time of surface wave attenuation.

Another method to determine the elasticity of a film that is spontaneously formed on a liquid surface was developed in

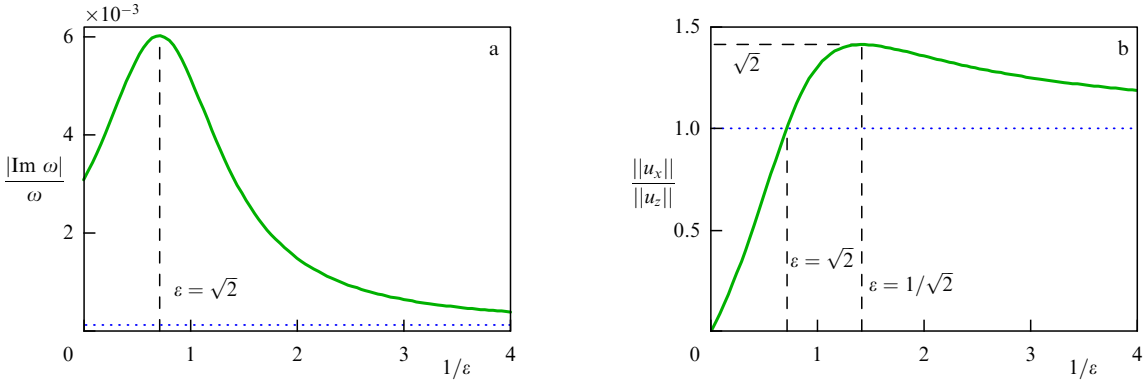

Figure 3. Dependence of (a) wave damping of surface waves (42) and (b) ratio of amplitudes of horizontal and vertical velocity components (43) on inverse value of dimensionless elastic modulus of film $1/\varepsilon$. Parameter γ is $\approx 1/120$, which corresponds to waves on water at frequency of 3 Hz. Blue dotted lines mark asymptotic form for a clean surface at $\varepsilon \to 0$.

Ref. [36]. The authors proposed to measure the horizontal and vertical velocities of wave motion on the liquid surface and analyze the ratio of their amplitudes $||u_i|| = \max_{x,y,t} |u_i|$. For a plane wave propagating in the x direction, we obtain

$$\frac{||u_x||}{||u_z||} \approx \frac{1}{\sqrt{\varepsilon^2 - \varepsilon\sqrt{2} + 1}}\,. \tag{43}$$

The ratio of the amplitudes varies in the range from 0 to $\sqrt{2}$, depending on the properties of the film (Fig. 3b). A combination of both methods allows us to eliminate possible ambiguity in determining the parameter ε when the corresponding equations have two solutions.

3.3 Nonlinear generation of slow current

We shall now consider the process of generation of a slow vortex current $\mathbf{V}$ that occurs because of the attenuation of surface waves. This is a quadratic effect in terms of wave amplitude; therefore, the characteristic frequency of the induced flow $\mathbf{V}$ is determined by the characteristic width $\Delta\omega$ of the spectrum of surface waves. We shall assume that this spectrum is narrow, $\Delta\omega \ll \omega$, so as to allow dividing relatively fast waves $\mathbf{u}$ and slow vortex flows $\mathbf{V}$ by frequencies.

Since the current $\mathbf{V}$ is incompressible, it can be parameterized by two components, for which we shall choose the vertical components of vorticity ϖ_z^{V} and velocity V_z, where $\boldsymbol{\varpi}^{\mathrm{V}} = \operatorname{rot}\mathbf{V}$. We now assume that the vortex flow $\mathbf{V}$ is weak and that the characterizing Reynolds number is small; hence, the dynamics of these two types of flow are linear and independent of each other. If $V_z = 0$, the streamlines of the slow flow are directed horizontally everywhere, and the incompressibility condition takes the form $\partial_\alpha V_\alpha = 0$. Below, in Section 3.5, we will show that the vertical flow V_z turns out to be suppressed. Therefore, here, we start with the calculations of the generation of vertical vorticity ϖ_z^{V}.

The equation for ϖ_z^{V} can be obtained from the z-component of the volume equation (37) and the boundary condition (38) as a result of linearization over the slow current $\mathbf{V}$ and retention of contributions quadratic in the wave amplitude, which are averaged over the rapid wave oscillations. However, the linear theory built in Section 3.2 turns out to be insufficient for the analysis of nonlinear terms. The point is that expressions (39) and (41) for the fields of velocity and vorticity are true only if the wave amplitude is small compared to the thickness of the viscous sublayer, $h \ll \delta$. In practice, the opposite case $\delta \ll h \ll 1/k$ is usually realized, and, therefore, the viscous sublayer should be measured from the current surface of the liquid [80] taking into account both its displacement and rotation relative to the plane $z = 0$. The mathematical aspect of this procedure is described in Appendix A. As a result, the vortex components of the velocity of wave motion in expressions (39) and (41) should be measured from the surface, which corresponds to the formal replacement $\exp(\varkappa z) \to \exp(\varkappa(z-h))$, and the horizontal components should now be understood as the corresponding projections of the vortex velocity onto the vectors tangential to the liquid surface.

As a result, the z-component of the vorticity equation (37) averaged over rapid wave oscillations takes the form

$$(\partial_t - \nu\Delta)\varpi_z^{\mathrm{V}} = \left\langle \varpi_\alpha^u\, \partial_\alpha(u_z - \partial_t h)\right\rangle. \tag{44}$$

The form of the nonlinear term on the right side of (44) is determined from Eqn (A2). The contribution to the right side proportional to $\partial_t\partial_\alpha h$ ensures that the rotation of the liquid surface is taken into account, which is accompanied by the rotation of the vector $\boldsymbol{\varpi}^u$, which in itself does not result in the generation of a mean flow. After averaging over rapid wave oscillations, the boundary condition (38) leads to

$$\partial_z\varpi_z^{\mathrm{V}} = -\epsilon_{\alpha\gamma}\left\langle(\partial_\alpha u_\beta + \partial_\beta u_\alpha)\partial_\beta\partial_\gamma h\right\rangle. \tag{45}$$

When calculating the average of the first term in (38), we took into account that the part of the vorticity $\boldsymbol{\varpi}^u$ linear in the wave amplitude has a zero projection onto the normal to the liquid surface. Note that the surface curvature appears on the right side, since $\partial_\beta\partial_\gamma h = -K_{\beta\gamma}$ in the linear order in the wave amplitude.

The right side of Eqn (44) is nonzero only in the viscous sublayer; therefore, we can say that a slow vortex current is generated in this sublayer. Since the characteristic horizontal scale of slow currents is significantly larger (not less than the wavelength), the system of Eqns (44) and (45) can be rewritten in the equivalent form

$$(\partial_z^2 - \hat{\varkappa}^2)\varpi_z^{\mathrm{V}} = 0\,, \qquad \rho\nu\,\partial_z\varpi_z^{\mathrm{V}}\big|_{z=0} = \epsilon_{\alpha\beta}\partial_\alpha\tau_\beta\,, \tag{46}$$

where the operator $\hat{\varkappa}^2 = \partial_t/\nu - \partial_\alpha\partial_\alpha$, and τ_α is the previously introduced virtual wave stress. After substituting relations for linear waves (44) and (45) into the right sides of expressions

(39) and (41), we obtain

$$\epsilon_{\alpha\beta}\partial_\alpha\tau_\beta = \rho\nu\epsilon_{\alpha\beta}\left\langle\frac{2}{k}(\partial_\alpha\partial_\gamma h)\big(\partial_\beta\partial_\gamma\partial_t(1-\hat{D})h\big) + (\partial_\alpha h)\big(\partial_\beta\partial_t\hat{D}\hat{\varkappa}h\big)\right\rangle, \tag{47}$$

where the operator $\hat{D}$ was determined earlier in expression (40), and the wave number k corresponds to waves at the frequency ω. In the limiting case of a free surface $\varepsilon \ll \sqrt{\gamma}$, in relation (47) it is necessary to take into account that $\hat{D}\hat{\varkappa} \simeq 2k$ and $|\hat{D}| \sim \gamma \ll 1$ and select the terms according to this small parameter. The expression for the stress $\boldsymbol{\tau}$ in this case was previously obtained, e.g., in Ref. [81, Eqn (7.154)]. In the opposite limit of a significant effect of the film $\varepsilon \gg \sqrt{\gamma}$, on the contrary, $\gamma \ll |\hat{D}| \leqslant 1$; therefore, only the second line in expression (47) should be retained. The formal solution to Eqn (46) is

$$\varpi_z^{\mathrm{V}} = \frac{\exp(\hat{\varkappa}z)}{\rho\nu\,\hat{\varkappa}}\,\epsilon_{\alpha\beta}\partial_\alpha\tau_\beta\,. \tag{48}$$

Note that the virtual wave stress (47) is a time-averaged quadratic form of h and, therefore, contains only small frequencies $\sim\Delta\omega$. The general case can be expanded into a direct sum of the result of pairwise interference of waves propagating at an angle of 2θ to each other [40]. This pair of waves generates the stress $\boldsymbol{\tau}$ with a wave number $q = 2k\sin\theta \leqslant 2k$. Based on (40), (42), and (47), it can be concluded that the absolute value of the virtual wave stress is $\tau \sim \operatorname{Im}\omega\cdot\rho\omega\langle h^2\rangle$. According to expression (48), the vorticity ϖ_z^{V} propagates to the depth $\sim\sqrt{\nu/\Delta\omega}$ if the time of change $1/\Delta\omega$ of the virtual wave stress is short compared to the time $t_E = 1/\nu q^2$ of viscous relaxation of the vortex flow. The amplitude of the flow is $V \sim \tau/(\rho\sqrt{\nu\Delta\omega})$. If the wave motion is almost monochromatic, $1/\Delta\omega \gg t_E$, the flow has vertical dependence $\exp(qz)$ and penetrates to a depth of $1/q$. An estimate for the flow amplitude is $V \sim \tau/(\rho\nu q)$. At the same wave motion $h(t,x,y)$, the right side of expression (47) increases by $1/\gamma$ under a transition from a clean surface to one with a film with $\varepsilon \gtrsim 1$. If the wave motion is monochromatic, the amplitude of vorticity (48) does not depend on viscosity in the case of a clean surface and is as large as $1/\gamma$ if $\varepsilon \gtrsim 1$.

3.4 Stokes drift and mass transport

To obtain the Lagrangian velocity averaged over wave oscillations, in addition to the Eulerian flow (48), we must calculate the Stokes drift (27). In the depth of the liquid outside the viscous sublayer, the Stokes drift is determined by the potential flow and, therefore, remains the same as in the nonviscous case [56]

$$U_\alpha^{\mathrm{S}} = \exp(2kz)\langle k^{-2}\partial_\beta h\,\partial_\alpha\partial_\beta\partial_t h + h\,\partial_\alpha\partial_t h\rangle\,, \tag{49}$$

and the vertical component is $U_z^{\mathrm{S}} \approx 0$.

Let us now find the correction to expression (49) that arises inside the viscous sublayer. This question is important in terms of the analysis of the motion of particles floating on the surface that have a small size compared to the thickness of the viscous sublayer. Since the viscous sublayer is measured from the current surface of the liquid, expression (27) must be modified according to the same scheme as expression (A2). More precisely, when determining the variation of the vortex component of the wave flow, the displacement of the Lagrangian trajectory must be measured from the liquid surface, i.e.,

$$V_i^{\mathrm{L}} = V_i + U_i^{\mathrm{S}}\,, \qquad U_i^{\mathrm{S}} = \big\langle G_{ij}^{\phi}(t,\mathbf{r}_0)\,\delta R_{1j}(t)\big\rangle + \big\langle G_{ij}^{\psi}(t,\mathbf{r}_0)\big(\delta R_{1j}(t) - \delta_{jz}h(t)\big)\big\rangle\,, \tag{50}$$

where G_{ij}^{ϕ} and G_{ij}^{ψ} are the gradients of the potential and vortex components of the velocity field (39) in a linear wave. Calculations by formula (50) on the surface lead to expression (49) with $z = 0$, where replacements $h \to (1-\hat{D})h$ must be made in the first term.

If the surface of the liquid is clean, $|D| \sim \gamma$, the correction to the result (49) that follows from the complete expression (50) is as small as γ and should be neglected. If the effect of the film on the surface motion is significant, $\varepsilon \gtrsim 1$ and $|D| \sim 1$, the Stokes drift is as small as at least γ compared to the Eulerian velocity (48); therefore, its consideration for the steady-state case would be an excess of accuracy. As a result, it turns out that the correction to the Stokes drift inside the viscous sublayer is insignificant and can be neglected in the future.

As with the tangential stress, the Stokes drift can be considered a result of the interference of two waves (see the text after expression (48)). Let us point out the characteristic differences between the Stokes drift and the slow Eulerian vortex flows generated by crossing waves. First, the penetration of the Stokes drift into the depth of the liquid can be described by the factor $\exp(2kz)$ and does not depend on the spatial configuration of the waves. Slow vortex flows can penetrate to a considerably greater depth determined by the factor $\exp(qz)$ with $q = 2k\sin\theta$ if the surface waves propagate at a small angle $2\theta \ll 1$ to each other [40]. Second, the Stokes drift on the surface is comparable to the steady-state Eulerian flow only in the case of a clean surface, $|D| \sim \gamma$, and for waves propagating at an angle $\sin(2\theta) \sim 1$ to each other. If the angle is small, $\theta \ll 1$, the amplitude of the Eulerian flow V increases by $\sim 1/\theta$ times, while the amplitude of the Stokes drift remains unchanged in order of magnitude. The surface film leads to an additional enhancement of the Eulerian flow. Third, the Stokes drift is an almost instantaneous (time of one oscillation period) response to the wave flow. This difference in dynamic properties from slow vortex currents manifests itself if the amplitude of surface waves changes at times that are considerably shorter than $t_E \sim 1/\nu q^2 = 1/(4\nu k^2\sin^2\theta)$. Not only is this realized for small angles 2θ between the waves [41] but it can also be observed for orthogonal surface waves if the characteristic time of attenuation and stabilization of wave motion turns out to be significantly less than the estimate $\sim 1/(\nu k^2)$ due to additional dissipation of the wave motion at the boundaries of the system or the presence of a surface film [37]. In this case, to interpret the motion of particles on the surface, it may be necessary to take into account the Stokes drift at initial times even if the surface of the liquid is covered with a film.

In our early work [35, 36], the vertical coordinate was not measured from the surface of the liquid to calculate the vortex component of the velocity in a linear wave. As a result, contributions arose in the individual Stokes drift and Eulerian velocity inside the viscous sublayer that were relatively large as $1/\gamma$ compared to the vortex correction given by expression (50). These contributions were equal to each other and had opposite signs; therefore, the total Lagrangian vorticity ϖ_z^{L} in the viscous sublayer coincided with the result of the calculations described above. The

method presented here is preferable, since it allows excluding immediately nonphysical contributions to both the Stokes drift and the Eulerian velocity. Otherwise, for a single plane traveling wave, it can be found that the Stokes drift vanishes on a clean liquid surface owing to the viscous correction [82]. Actually, even in the limit of an almost incompressible film $\varepsilon \to \infty$, the Stokes drift for a traveling wave on the surface decreases by only two times compared to the case of a clean surface and does not vanish. This, however, has no physical meaning in our formulation of the problem, since the Stokes drift is comparable to the Eulerian flow established in just one period of oscillations under the action of a virtual wave stress, which is now estimated to be $\sim 1/\gamma$ times greater than expression (16).

If the wave motion is significantly three-dimensional, there is no direct generalization of relation (29) between the surface density of the momentum π_α and the vertically integral Stokes drift. Indeed,

$$\pi_\alpha = \rho \left\langle \int_{-\infty}^{h} \mathrm{d}z\, v_\alpha \right\rangle \approx \rho k^{-1} \langle h\, \partial_\alpha \partial_t h \rangle\,; \tag{51}$$

therefore, the difference between these two quantities is the circulation flow:

$$\pi_\alpha - \int_{-\infty}^{0} \mathrm{d}z\, U_\alpha^{\mathrm{S}} = \frac{1}{4k}\, \epsilon_{\alpha\beta} \partial_\beta \langle \epsilon_{\gamma\delta} \partial_\gamma h\, \partial_\delta \partial_t h \rangle\,. \tag{52}$$

The difference results from the fact that, in the general case, the Lagrangian trajectories in the wave field are significantly three-dimensional (we recall that these trajectories are almost closed in one period). As a result, the flows of the liquid and Lagrangian particles across a single vertically oriented rectangular elementary area do not coincide. The reason is that, at the edges of the elementary area, there are trajectories that intersect it only in one direction during one oscillation period, and they return beyond the edge of the elementary area. In the case of a plane wave (29), this edge effect occurs only at the horizontal boundaries of the elementary area; therefore, it is eliminated by vertical integration. In the case of significantly three-dimensional wave motion, the edge effect also arises at the vertical boundaries of the elementary area; therefore, it cannot be eliminated by vertical integration in (52).

3.5 Vertical current

We shall now return to the component of the slow current that has $V_z \neq 0$. To derive the boundary condition, let us formally integrate the continuity equation $\operatorname{div} \mathbf{v} = 0$ vertically and average the result over the rapid wave oscillations:

$$\left\langle \int_{-\infty}^{h} \partial_\alpha v_\alpha \, \mathrm{d}z \right\rangle + \langle v_z|_{z=h} \rangle = 0\,. \tag{53}$$

In the first term, we factor the derivative outside the integral sign using the rule of differentiation of integrals with a variable upper limit. Moreover, we transform the second term according to the kinematic boundary condition (32)

$$\frac{\partial_\alpha \pi_\alpha}{\rho} + \partial_\alpha \left\langle \int_{-\infty}^{h} V_\alpha \, \mathrm{d}z \right\rangle + \langle \partial_t h \rangle = 0\,. \tag{54}$$

Within an accuracy to the second order in wave amplitude, the upper limit of integration in the second term can be assumed to be zero, and, taking into account the incompressibility of the slow flow $\operatorname{div} \mathbf{V} = 0$, we find the final answer:

$$V_z\big|_{z=0} = \frac{\partial_\alpha \pi_\alpha}{\rho} + \partial_t \langle h \rangle\,. \tag{55}$$

This boundary condition is a clarification of the boundary condition (19) for the vertical velocity that was used earlier.

Let us estimate the right side of expression (55). First, we recall that the nonlinear interaction of surface waves can generate a slow potential flow $\langle \mathbf{u} \rangle$, which we discussed earlier in Section 2.4. According to the results of this section, in the case of an ideal liquid, the right side should be estimated as $\sim \Delta\omega\, k \langle h^2 \rangle$, i.e., it has smallness in the spectral width of the waves. Second, in addition to the excitation of a slow potential flow, the excitation of a slow vortex contribution with $V_z \neq 0$ is also possible. For this contribution, the right side either has a similar smallness in spectral width or, if taking into account weak attenuation of waves $\partial_\alpha \pi_\alpha / \rho \sim \operatorname{Im}\omega\, k \langle h^2 \rangle$, contains another smallness — the inverse quality factor of a wave (42). Hence, the boundary conditions for V_z (55) and ϖ_z^{V} (46) differ in type, while the volume equation for V_z coincides with that for ϖ_z^{V}. As a result, an estimate for V_z will be the right side of expression (55), which is always small compared to the velocity of the Stokes drift on the surface $\sim \omega k \langle h^2 \rangle$ as either $\Delta\omega/\omega \ll 1$ or $\operatorname{Im}\omega/\omega \ll 1$.

The suppression of currents with $V_z \neq 0$ is confirmed in experiments. The existence of a nonzero vertical flow means the compressibility of the surface flow, since the two-dimensional divergence of the Lagrangian velocity is $\partial_\alpha V_\alpha^{\mathrm{L}} \neq 0$. In the experimental work [14], it was observed that the two-dimensional divergence of the velocity is small compared to the vertical vorticity ϖ_z^{L}, indicating the relative smallness of the vortex flow with $V_z \neq 0$ according to the above reasoning.

As discussed earlier, the attenuation of a traveling wave gives rise to the virtual wave stress $\tau = \operatorname{Im}\omega\, \rho\omega H^2$ (see expression (16)). The stress τ causes a flow that carries along the material of the film. If there are surface boundaries that impede the motion of the film, its reaction occurs, limiting its further extension and compression. The reaction leads to the suppression of the vortex flow under the film. However, at high wave amplitudes, the stress τ can lead to a rupture of the film; therefore, it is carried along by the flow from the part of the surface, resulting in spatial non-uniformity in the properties of the surface [83]. In particular, this non-uniformity can give rise to a vertical component of the velocity in the wave-induced vortex flow $\mathbf{V}$. These scenarios, however, are beyond the scope of our analysis.

3.6 Discussion of experiments

We are now ready to discuss experiments in which surface vortex currents were generated by crossing waves. The first studies investigated the generation of flows by two orthogonal standing waves in square cells. The waves could be excited either by oscillations of the meniscus at the walls of the cell resulting from its periodic vertical motion [12] or, e.g., by vertically oscillating plungers mounted on the lateral walls [37]. The deviation of the liquid surface from equilibrium in this system can be described by the expression

$$h = H_1 \cos(\omega t) \cos(kx) + H_2 \cos(\omega t + \psi) \cos(ky)\,, \tag{56}$$

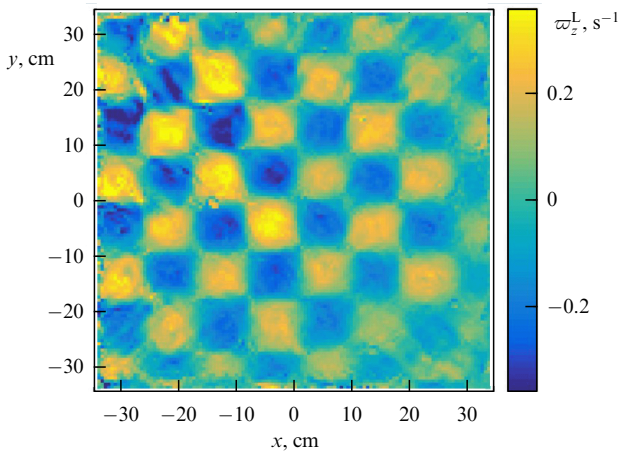

Figure 4. Distribution of vertical component of vorticity of vortex motion generated by two orthogonal standing waves (see expression (57)); wave frequency is 3 Hz, phase difference is $\psi = \pi/2$, and angular amplitude is $kH = 0.035$. (Data taken from experiment [13].)

where ψ is the phase shift between the waves. For simplicity, the depth of the liquid will be assumed to be infinite. Slow currents can be experimentally characterized by vertical vorticity from the Lagrangian velocity $\varpi_z^{\mathrm{L}} = \varpi_z^{\mathrm{V}} + \epsilon_{\alpha\beta}\,\partial_\alpha U_\beta^{\mathrm{S}}$, for which it follows from expressions (48) and (49) in the steady-state regime [36] that

$$\varpi_z^{\mathrm{L}} = -\left[\frac{\varepsilon^2 \exp\left(kz\sqrt{2}\right)}{2\gamma(\varepsilon^2 - \varepsilon\sqrt{2} + 1)} + \sqrt{2}\exp\left(kz\sqrt{2}\right) + \exp\left(2kz\right)\right] \times H_1 H_2 \omega k^2 \sin\left(kx\right)\sin\left(ky\right)\sin\psi\,. \tag{57}$$

Here, the last term in parentheses corresponds to the Stokes drift, and the first two terms describe the contribution of the Eulerian flows. The contributions have different dependences on the depth z but the same spatial structure in the horizontal plane. The first term in brackets describes the effect of the surface film, and it dominates if $\varepsilon \gg \sqrt{\gamma}$. In the opposite case of an almost clean surface $\varepsilon \ll \sqrt{\gamma}$, it can be neglected. Then, the vorticity ϖ_z^{L} measured in the steady-state regime does not depend on the viscosity of the liquid. An experimental observation of the vorticity distribution is shown in Fig. 4.

From an experimental viewpoint, it is easiest to measure flows on the surface of a liquid at $z = 0$. In Ref. [12], a 'chessboard' of vortices corresponding to $\varpi_z^{\mathrm{L}} \propto \sin(kx) \times \sin(ky)$ was observed, and it was shown that the generation of slow currents was a quadratic effect in terms of the wave amplitude, $\varpi_z^{\mathrm{L}} \propto H_1 H_2$. To explain the experimental results, a theory was developed that described the generation of Eulerian vorticity for a clean surface; however, the contribution from the Stokes drift was not taken into account. On the contrary, in Refs [14, 15], the authors explained the generation of the 'chessboard' of vortices by the Stokes drift and did not consider the viscous mechanism of current generation. In those studies, the experimental setup allowed changing the phase difference ψ between the waves. However, at small values of ψ, large-scale flows arose in the system, which significantly deformed the vortex lattice. The dependence $\varpi_z^{\mathrm{L}} \propto \sin\psi$ was confirmed quantitatively in Ref. [13], where measurements were not carried out in the steady-state regime, and, therefore, large-scale flows deforming the vortex lattice did not have time to be excited.

To achieve quantitative agreement between theory and experiment, it was necessary to take into account both mechanisms of current generation and the effect of a thin adsorbed film on the surface [35, 36]. The corresponding theory was tested experimentally in Ref. [37], where the existence of the Eulerian contribution ϖ_z^{V} to the slow current was proven experimentally. The idea was that surface waves attenuated considerably faster than slow flows due to the presence of a film on the surface and friction against the boundaries. Therefore, after switching off the pumping, it was possible to observe a 'chessboard' of vortices even in the complete absence of wave motion. Nonstationary processes of vorticity establishment and attenuation were also theoretically described and experimentally studied in Ref. [37]. Another idea that allowed verifying the existence of the Eulerian contribution ϖ_z^{V} to the Lagrangian vorticity ϖ_z^{L} was to investigate the dependence of the intensity of slow currents on depth. The corresponding measurements were carried out in Ref. [16], and their results were interpreted by the authors in favor of the existence of both contributions: Eulerian vorticity and Stokes drift.

A further development was related to the study of systems where waves propagated at an arbitrary angle to each other. Let two traveling waves propagate at angles $\pm\theta$ to the y-axis; therefore, the surface has the shape

$$h = H_1 \cos\left(\omega t - \mathbf{k}_1\mathbf{r}\right) + H_1 \cos\left(\omega t - \mathbf{k}_2\mathbf{r}\right) \tag{58}$$

with the wave vectors $\mathbf{k}_{1,2} = k(\pm\sin\theta, \cos\theta)$. Then, at an unlimited depth of the liquid, the vorticity established at long times is

$$\varpi_z^{\mathrm{L}} = -\left(\frac{\varepsilon^2 \exp\left(qz\right)\cos\theta}{\sqrt{2}\gamma(\varepsilon^2 - \varepsilon\sqrt{2} + 1)} + 4\exp\left(qz\right)\cos^3\theta + 4\exp\left(2kz\right)\cos^3\theta\sin\theta\right) H_1 H_2 \omega k^2 \sin\left(qx\right), \tag{59}$$

where the wave number that determines the period of modulation is $q = 2k\sin\theta$. If the angle between the waves is small, the waves are able to generate a large-scale current that has a long relaxation time [40, 41]. This scenario enabled an explanation of the generation of large-scale flows at long times observed in many early experiments. Recent investigations have focused on the result of interference of many waves at a time [18–20]. Complex wave motion makes it possible to create controllably vortex flows on a surface with complex geometry. If there are particles on the surface of a liquid, they are drawn into motion by vortex structures, and their motion can be controlled by tuning the wave field. This paves the way to applications related to the manipulation and sorting of particles. When $\theta \to 0$, proportionality between (42) and the Eulerian part of the vorticity in (59) as functions of ε is reached, which corresponds to the qualitative understanding that currents are generated due to wave attenuation.

4. Interaction of waves with near-surface currents

As the intensity of the vortex flow **V** increases, its interaction with the wave motion becomes significant. As a result, on the one hand, deformation of the wave field by the vortex flow gives rise to a volume force $\mathbf{f}^{\mathrm{V}}$ that acts on the flow **V** from the side of the waves; it is called the vortex force [57]. On the other hand, the waves begin to scatter and refract on the vortex

flow. As a result, the force $\mathbf{f}^{\mathrm{V}}$ gets additional correlations with the flow $\mathbf{V}$, which can significantly modify its dynamics. This occurs, e.g., in the case of Langmuir circulation (see below). The interaction between waves and a vortex flow does not depend on the fact that the liquid has low viscosity. Hence, it is sufficient to describe this interaction within the model of an ideal liquid.

The separation into wave motion and a vortex flow is possible if there is a separation of these flows in time, that is, the wave frequency ω is high compared to both the rate of change $1/T$ of the flow $\mathbf{V}$ and the characteristic value of its gradient $\operatorname{grad}\mathbf{V} \sim V/L$,

$$\frac{1}{\omega T} \ll 1\,, \qquad \frac{V}{L\omega} \ll 1\,, \tag{60}$$

where L is the characteristic scale of the change in the flow. In particular, this means that the Froude number that characterizes the vortex flow is small, $\mathrm{Fr} = V^2/gL \ll 1$. This inequality allows us to assume that the boundary condition (19) is also preserved for the vertical component V_z, i.e., the vortex flow $\mathbf{V}$ does not lead to a change in the shape of the surface.

4.1 Vortex force

As with the virtual tangential stress $\boldsymbol{\tau}$, the vortex force $\mathbf{f}^{\mathrm{V}}$ arises since the wave flow is no longer completely potential. The nonzero high-frequency vorticity $\boldsymbol{\varpi}^u$ in the bulk arises because the wave field is deformed by the nonzero vorticity $\boldsymbol{\Omega} = \operatorname{rot}\mathbf{V}$ of the vortex flow. To find $\boldsymbol{\varpi}^u$, let us represent the wave flow as a potential part and a small vortical correction $\mathbf{u}^{\varpi}$, $\mathbf{u} = \operatorname{grad}\phi + \mathbf{u}^{\varpi}$. The equation for vorticity (37) linearized in the wave amplitude and the amplitude of the small vortex correction has the form [56]

$$\bigl(\partial_t + (\mathbf{V}\nabla)\bigr)\boldsymbol{\varpi}^u = \operatorname{rot}\left[\operatorname{grad}\phi \times \boldsymbol{\Omega}\right], \qquad \boldsymbol{\varpi}^u = \operatorname{rot}\mathbf{u}^{\varpi}\,. \tag{61}$$

In Eqn (61), we have disregarded the viscous term, since the scale of the flow $\boldsymbol{\varpi}^u$ in the bulk is assumed to be considerably larger than the viscous scale δ, and the term $(\boldsymbol{\varpi}^u\nabla)\mathbf{V}$, since it is relatively as small as $V/L\omega$ compared to the term $\partial_t\boldsymbol{\varpi}^u$. The solution of (61) is

$$\begin{aligned} &\boldsymbol{\varpi}^u = \operatorname{rot}\left[\delta\mathbf{R}_1 \times \boldsymbol{\Omega}\right],\\ &\delta\mathbf{R}_1(t,\mathbf{r}) = \int^t \mathrm{d}t'\operatorname{grad}\phi\bigl(t',\mathbf{r}(t')\bigr)\,, \end{aligned} \tag{62}$$

where the Lagrangian trajectory $\mathbf{r}(t)$ is given by the slow flow, $\dot{\mathbf{r}}(t) = \mathbf{V}(t,\mathbf{r})$, and $\delta\mathbf{R}_1$ is the displacement of the Lagrangian marker introduced in (27), resulting from wave oscillations. An estimate of the vorticity amplitude (62) is $\varpi^u \sim hV/L$, i.e., the vortex part of the wave oscillating motion $\mathbf{u}^{\varpi}$ is relatively small in the second parameter (60), $u^{\varpi}/u \sim V/L\omega$.

In order to obtain a generalization of Eqn (17) for the slow current $\mathbf{V}$ with respect to the influence of waves, one should extract in (30) the term bilinear in $\operatorname{grad}\phi$ and $\boldsymbol{\varpi}^u$. Then, the term should be averaged over fast oscillations. Detailed calculations are presented in Appendix B. We write the resulting Navier–Stokes equation in the Lamb form [56],

$$\partial_t\mathbf{V} + \left[\boldsymbol{\Omega} \times (\mathbf{V} + \mathbf{U}^{\mathrm{S}})\right] = -\frac{\nabla\overline{\mathcal{P}}}{\rho} + \nu\Delta\mathbf{V}\,. \tag{63}$$

If we move the term proportional to the Stokes drift to the right-hand side of Eqn (63), we obtain the vortex force $\mathbf{f}^{\mathrm{V}} = \rho[\mathbf{U}^{\mathrm{S}} \times \boldsymbol{\Omega}]$. The form of the nonlinear term in (63) can be interpreted as follows: the vorticity in the vortex flow is transferred by not only the flow itself but also the Stokes drift generated by the wave motion, i.e., on the whole, with the average Lagrangian velocity. The effective pressure $\overline{\mathcal{P}}$ in (63) differs from the physical pressure (see (B4)). It must be determined from the condition of flow incompressibility $\operatorname{div}\mathbf{V} = 0$ and the condition that the vertical velocity V_z is zero on the surface.

Which effect determines the vortical flow $\mathbf{V}$ — the virtual wave stress $\boldsymbol{\tau}$ or the vortex force $\mathbf{f}^{\mathrm{V}}$ — depends on its amplitude. The virtual wave stress is estimated as $\tau \sim \operatorname{Im}\omega\,\omega H^2$, where the wave decay rate is given in (42). The volume force is estimated as $f^{\mathrm{V}}/\rho \sim \omega k H^2\Omega$ and penetrates to a depth of $\sim 1/k$, assuming the vertical scale of the slow flow is greater than or of the order of the wavelength. The effects are of the same order when the vorticity of the slow flow is comparable to the wave decay rate,

$$\int_{-\infty}^{0} \mathrm{d}z\, f^{\mathrm{V}} \sim \tau: \qquad \Omega \sim \operatorname{Im}\omega\,. \tag{64}$$

At lower velocity amplitudes, the effect produced by $\boldsymbol{\tau}$ dominates, while at higher amplitudes, the effect produced by the force $\mathbf{f}^{\mathrm{V}}$ dominates. Estimate (64) is rough and may require refinement for specific flow geometries.

4.2 Wave propagation on background of vortical flow

Let us now consider how the vortical flow affects wave propagation. The vorticity $\boldsymbol{\varpi}^u$ found above describes the local distortion of the wave field produced by the presence of the vortical flow $\mathbf{V}$. Our goal now is to derive a system of equations for the potential ϕ and the surface form h that determines wave propagation in the linear approximation with respect to their amplitude. Throughout, we will disregard viscosity. We start from the Euler equation for the wave motion $\mathbf{u}$ on the background of the vortical flow $\mathbf{V}$:

$$\partial_t\mathbf{u} + (\mathbf{u}\nabla)\mathbf{V} + (\mathbf{V}\nabla)\mathbf{u} = -\frac{\nabla P^u}{\rho} + \mathbf{g}\,, \tag{65}$$

where P^u is the part of the pressure associated with the wave motion. The vorticity $\boldsymbol{\varpi}^u$ itself does not uniquely determine the vortical part of the wave field $\mathbf{u}^{\varpi}$. We fix this ambiguity by imposing the condition on the surface $u_z^{\varpi}|_{z=0} = 0$ (deep down, the entire $\mathbf{u}^{\varpi}$ vanishes); as a result, the change in the surface shape turns out to be related only to the potential part of the wave flow. We generalize the Bernoulli equation (2) to the form [58]

$$\frac{P^u}{\rho} = -gz - (\partial_t + V_i\partial_i)\phi + p^{\varpi}\,, \tag{66}$$

where p^{ϖ} can be conventionally called the contribution to the pressure from the vortical part of the flow $\mathbf{u}^{\varpi}$. The kinematic (2) and dynamic (33) boundary conditions take the form

$$(\partial_t + \partial_\alpha V_\alpha)h = \hat{k}\psi\,, \tag{67}$$

$$(\partial_t + V_\alpha\partial_\alpha)\psi = -\varepsilon_{\hat{k}}h + p^{\varpi}\,, \tag{68}$$

where $\varepsilon_{\hat{k}} = g + (\sigma/\rho)\hat{k}^2$ is the wave potential energy operator, ψ is the value of the potential ϕ on the surface $z = 0$, and the quantities V_α and p^{ϖ} should also be taken there. The volume equation for p^{ϖ} can be obtained by substituting the

ansatz (66) into equation (65), and the boundary condition for p^{ϖ} on the surface follows from the requirement $u_z^{\varpi} = 0$:

$$\Delta p^{\varpi} = \partial_i \phi \, \Delta V_i + 2 \partial_j u_i^{\varpi} \, \partial_i V_j \,, \tag{69}$$

$$\partial_z p^{\varpi}\big|_{z=0} = \partial_\alpha \psi \, \partial_z V_\alpha \,, \quad p^{\varpi}\big|_{z\to-\infty} \to 0 \,. \tag{70}$$

If the slow flow $\mathbf{V}$ is purely potential, i.e., it represents a long surface wave, then $\Delta \mathbf{V} = 0$ and $\mathbf{u}^{\varpi} = 0$, so $p^{\varpi} = 0$ as well. It follows that the pressure part p^{ϖ} is a product of the vorticity $\boldsymbol{\Omega}$ of the slow flow, but this relationship is nonlinear in $\mathbf{V}$.

4.3 Guyon waves

The Guyon wave is a plane wave traveling along the x-axis, propagating on a background of a flow $V_x(z)$ directed along the same axis and having a vertical shear (see, e.g., [59]). We will demonstrate how the equations from Section 4.2 allow us to determine the properties of Guyon waves to the first order in the small parameter $\Omega_y/\omega \ll 1$, where the vorticity of the slow flow is $\Omega_y = \partial_z V_x$. In doing so, we will reproduce the classical result of [60].

In the leading order of the wave amplitude, the surface elevation amplitude and the potential are harmonic functions. We represent them using complex amplitudes:

$$h = H \exp(\mathrm{i}\varphi) \,, \quad \phi = \psi \exp(kz) \,, \quad \psi \propto \exp(\mathrm{i}\varphi) \,, \tag{71}$$

where the phase is $\varphi = kx - \omega t$. For example, $\operatorname{Re} h$ is the physical surface elevation amplitude. Without loss of generality, the wave amplitude H can be considered positive.

The Stokes drift is given by expression (28), so the only nonzero component of the vortex force is the vertical one, $f_z^{\mathrm{V}} = k\omega H^2 \exp(2kz)$. This force contributes only a time-independent component to the pressure and does not alter the slow flow.

Let us now determine the dispersion relation. First, note that, due to the geometry of the problem, $\varpi^u = 0$. The boundary conditions (67) and (68) on the surface are

$$(-\mathrm{i}\omega + \mathrm{i}kV_x)h = k\psi \,, \tag{72}$$

$$(-\mathrm{i}\omega + \mathrm{i}kV_x)\psi = -gh + p^{\varpi} \,, \tag{73}$$

and the vortical pressure correction is

$$p^{\varpi}(0) = 2\mathrm{i}k\psi \left(V_x(0) - 2k \int_{-\infty}^{0} \mathrm{d}z \exp(2kz) V_x(z) \right) . \tag{74}$$

Solving equations (72), (73) in the linear approximation with respect to the small parameter $\Omega_y/\omega \ll 1$ yields the dispersion relation [60]

$$\omega = \sqrt{gk} + \omega' \,, \qquad \omega' = 2k^2 \int_{-\infty}^{0} \mathrm{d}z \, \exp(2kz) V_x(z) \,. \tag{75}$$

If the shear force is constant along the vertical, $V_x = \Omega_y z$, then the frequency shift is $\omega' = -\Omega_y/2$.

4.4 Short-wave limit

The short-wave limit is reached when the scale L of the flow $\mathbf{V}$ significantly exceeds the wavelength, $kL \gg 1$. In the region of wave propagation, it should be assumed that the change in the velocity V in order of magnitude does not exceed the phase velocity of the wave ω/k. Then, the second term in (69) is, at most, of the same order as the first, and, in the boundary condition (68), p^{ϖ} is smaller than $\phi \, \partial_\alpha V_\alpha$ by a factor of $1/kL$. Neglecting this small correction, we arrive at the wave equation

$$\varepsilon_{\hat{k}} (\partial_t + V_\alpha \partial_\alpha) \frac{1}{\varepsilon_{\hat{k}}} (\partial_t + \partial_\beta V_\beta) \psi = -\omega_{\hat{k}}^2 \psi \,, \tag{76}$$

where ψ is the value of the potential on the surface, and the dispersion relation is $\omega_k = \sqrt{gk + (\sigma/\rho)k^3}$.

Let us consider the propagation of wave packets using the standard geometrical optics approximation. We will treat ψ as a complex amplitude and parameterize it via the absolute amplitude value $|\psi|(t,x,y)$ and the real phase (eikonal) $\varphi(t,x,y)$, $\psi = |\psi| \exp(\mathrm{i}\varphi)$. The amplitude $|\psi|(t,x,y)$, the wave vector $\mathbf{k} = \operatorname{grad} \varphi$, and the frequency $\omega = -\partial_t \varphi$ are slowly varying quantities compared to the phase φ. The real part of equation (76) multiplied by $\exp(-\mathrm{i}\varphi)$, where corrections of order $1/(kL)^2$ are neglected, yields the dispersion relation

$$\big(\omega - (\mathbf{V}\mathbf{k})\big)^2 = \omega_k^2 \,. \tag{77}$$

The combination $\widetilde{\omega} = \omega - (\mathbf{V}\mathbf{k})$ is the relative frequency of the wave — the frequency of its oscillations in the reference frame moving with the fluid velocity $\mathbf{V}$ — whereas ω is the wave frequency in the stationary frame. In other words, relation (77) includes the Doppler effect. Let us compute the derivatives of the dispersion relation (77) with respect to time and coordinates, which results in equations for the evolution of the frequency and the wave vector along the motion of the wave packet:

$$\Big(\partial_t + \big((\mathbf{V} + \mathbf{v}^{\mathrm{g}})\nabla\big)\Big)\omega = (\mathbf{k}\,\partial_t \mathbf{V}) \,, \tag{78}$$

$$\Big(\partial_t + \big((\mathbf{V} + \mathbf{v}^{\mathrm{g}})\nabla\big)\Big)k_\alpha = -k_\beta \, \partial_\alpha V_\beta \,, \tag{79}$$

where the group velocity of the packet relative to the fluid is $v_\alpha^{\mathrm{g}} = \partial\omega_k/\partial k_\alpha$. In the stationary coordinate system, the wave packet moves with velocity $\mathbf{V} + \mathbf{v}^{\mathrm{g}}$. The first equality (78) implies, notably, that, in a stationary flow $\mathbf{V}$, the wave frequency ω in the stationary frame remains constant. The second equation (79) determines the trajectory of the wave packet propagation.

The equation for the wave amplitude follows from the imaginary part of equation (76) multiplied by $\exp(-\mathrm{i}\varphi)$. It can be reduced to the form of a conservation law

$$\partial_t \mathcal{I} + \operatorname{div}\big((\mathbf{V} + \mathbf{v}^{\mathrm{g}})\mathcal{I}\big) = 0 \,, \qquad \mathcal{I} = \frac{\varepsilon_k H^2}{2\omega_k} \,, \tag{80}$$

where the surface oscillation amplitude is $H = (k/\omega_k)|\psi|$. To derive (80), corrections linear in the derivatives of the slowly varying quantities $\mathbf{V}$, $|\psi|$, ω, $\mathbf{k}$ must be retained on both sides of the wave equation (76). This procedure is carried out in Appendix B. The quantity $\mathcal{I}$ is proportional to the surface energy density of the wave $\varepsilon_k H^2/2$, divided by its relative frequency ω_k. The conserved quantity $\int \mathrm{d}x \, \mathrm{d}y \, \mathcal{I}$ is called the wave action (see, for example, [61] and monographs [62, 84, 85]).

Based on the presented theory, let us consider the problem of a gravity wave propagating against a current $V_x(x) < 0$ that is inhomogeneous along the streamlines, when a plane wave propagates in the positive x direction relative to the fluid, i.e., $k_x > 0$. The dispersion relation (77) takes the form $k_x(V_x + 2v^{\mathrm{g}}) = \omega$, where $v^{\mathrm{g}} = \omega_k/2k_x$, which can be treated as an equation for the wave number k_x [63, 64]. Assume the

wave is stationary, so that $\partial_t \mathcal{I} = 0$ in (80). Then, the wave amplitude satisfies the relation $v^g(V_x + v^g)H^2 = \text{const}$. It increases unlimitedly when approaching the stopping point $V_x = -v^g$. At this point (assume its coordinate is $x = 0$), the group velocity becomes half of its value $v^{g0} = g/2\omega$ in the region where there is no flow, $v^g = v^{g0}/2$ (or $k_x = 4k_x^0$).

Near the stopping point, the equation for k_x presented above leads to the speed of the wave packet in the absolute coordinate system behaving as the square root of the distance to this point, $V_x + v^g \propto \sqrt{|x|}$. Consequently, there is an unbounded growth in wave steepness according to the law $kH \propto |x|^{-1/4}$. If its initial amplitude is sufficiently large, this growth leads to wave breaking, so that beyond the point $V_x = -v^{g0}/2$ the water surface becomes smooth. The disappearance of the wave leads to the transfer of its momentum to the flow, which is observed in experiments [86]. There are also oceanic measurements where increased wave breaking density was observed in regions of strong upwelling currents, which lead to large gradients in horizontal flow velocity [87]. The stopping point $V_x = -v^g$ corresponds to the merging of two roots of the equation for k_x. Therefore, for a sufficiently small initial wave amplitude, when breaking does not occur, a reflected wave with $k_x > 4k_x^0$ is generated, whose group velocity $v^g < -V_x$, and which is consequently carried by the flow in the negative x direction. For a mathematical description of wave behavior near the reflection point $x = 0$, it is necessary to go beyond the geometrical optics approximation (77) and return to the original wave equation (76). In [64], based on asymptotic analysis, it was established that it takes the form of an Airy equation. The wave equation (76) we obtained allows a systematic transition to this limit.

4.5 Langmuir circulation

The concept of vortex force has made it possible to explain the mechanisms behind the generation and maintenance of Langmuir circulation [88]. Langmuir circulation arises on a water surface when two conditions coincide: a propagating (along the x-axis) surface wave (7) is excited, and a wind-induced flow $V_x^0(z)$ with vertical shear is established in the direction of its propagation (or at a small angle to it). Langmuir circulation $\mathbf{V}$ is a superposition of two flow components, which are almost uniform along the x-direction and quasi-periodic in the transverse y-direction. The first component is a modulation $\delta V_x(y,z)$ of the shear flow $V_x^0(z)$, and the second component consists of rolls with circulation in the transverse plane yz, in which the velocity can be parameterized by a stream function $\Psi(y,z)$: $\delta V_y = \partial_z \Psi$, $\delta V_z = -\partial_y \Psi$. The flow within the rolls leads to the accumulation of foam and contamination on the liquid surface into stripes elongated along the x-direction, which visualizes the Langmuir circulation. Furthermore, the vertical velocity component in the rolls enhances turbulent mixing in the upper oceanic layer (see, for example, the general review [89] and the review of recent experimental work with the Black Sea [90]).

Study [65] demonstrated that a combination of a propagating wave and a shear flow is unstable with respect to transverse modulation. The structure of the unstable mode corresponds to Langmuir circulation. In this problem, besides the conditions of weak shear flow $\Omega = \partial_z V_x^0$ and small wave amplitude $kH \ll 1$, an important dimensionless parameter is the Langmuir number $\mathrm{La} = v^2 k^2/\omega H^2 \Omega$, where viscosity is often interpreted as turbulent viscosity. If $\mathrm{La} \ll 1$, the viscosity does not play a significant role in the dynamics of the unstable mode. In this limit, specifically, the growth rate of the instability found in [65] for the case of a vertically uniform shear flow ($\Omega_y^0 = \partial_z V_x^0$ independent of the vertical) is

$$\lambda = \sqrt{2\Omega_y^0 \omega}\, \frac{kH\theta}{\mu}\,, \tag{81}$$

where $2\pi/(k\theta)$ is the modulation period in the y-direction, μ is the smallest root of the equation $J_\theta(\mu) = 0$, and J is the Bessel function. It should be assumed that the shear force Ω_y^0 significantly exceeds the value (19) produced by wave damping; then, it also exceeds the instability growth rate, $\lambda \ll \Omega_y^0$. Note also that the instability occurs only if the shear is co-directional with the wave, $\Omega_y^0 > 0$ [91]. If the modulation period is large compared to the wave period, $\theta \ll 1$, then the longitudinal vorticity $\delta\Omega_x$ penetrates to a depth of $\sim 1/k$, whereas the circulation $\delta V_{y,z}$ and the modulation of the shear flow δV_x penetrate to a greater depth, $\sim 1/k\theta$. The velocity amplitude in the circulation is significantly weaker than the amplitude of the shear modulation, $\delta V_{y,z}/\delta V_x \sim \lambda/\Omega_y^0$. The described mechanism for the generation of Langmuir circulation was subsequently named the CL2-model after the authors A.D.D. Craik and S. Leibovich.

Model [65] does not account for wave dynamics, and therefore the Stokes drift in it is determined solely by the original (reference) wave (7). However, the periodic modulation of the vortical flow in the y-direction also leads to a similar modulation of the wave motion. This modulation has been observed both in numerical simulations [92, 93] and in experiments [94]. The interference between the base wave and the modulated wave results in a modulation of the Stokes drift, which in turn alters the dynamics of the vortical flow. Thus, the modulated wave becomes the third component of the unstable mode. Theoretical study [58] takes into account the wave modulation. The instability growth rate does not change significantly in the region $\theta \gtrsim 1$, since, in this case, the wave vector of the scattered wave differs substantially from k, i.e., it does not satisfy the dispersion relation. Weak wave modulation in this limit was studied in [95]. For large modulation periods, wave scattering becomes more significant, so that for $\theta \ll (\Omega_y^0/\omega)^{1/2}$ the instability growth rate becomes independent of the modulation period, $\lambda = \Omega_y^0 kH$. Note that, in the course of the calculations, the vortical pressure correction p^ϖ in the boundary condition (73) turns out to be the key one; that is, one can say that p^ϖ takes into account the scattering of the reference wave. However, it should be remembered that, for wave scattering to produce a coherent effect, the spatial structure of the Langmuir circulation must be periodic with long-range order, persisting over distances of the order of the wave travel length in a time of $\sim 1/\lambda$. In reality, this condition is apparently not always met. Also noteworthy are earlier papers [56, 96], which showed that two waves propagating at angles equal in magnitude but opposite in sign relative to the shear flow lead to a linear growth in time of the Langmuir circulation when its amplitude is small and to the maintenance of the circulation in a state of saturated amplitude due to turbulent viscosity. This mechanism for generating circulation is called CL1.

5. Turbulent regime

In a number of experiments [21–25], in which surface waves were excited by the mechanism of Faraday instability, and in

experiments [53, 54], in which waves in a square cell were excited by plungers located on adjacent walls, slow vortex flows generated by waves exhibited a turbulent character near the surface. Their statistical properties reproduced a number of features found in two-dimensional turbulence. For the sake of simplicity, Appendix C briefly presents the main properties of a two-dimensional turbulent flow. To learn more about the features of two-dimensional turbulence, we recommend review [55].

The turbulent nature of a flow generated by Faraday waves was first studied in Ref. [21]. The experiment was carried out in shallow water; the thickness of the liquid was ≈ 2 mm, and the wavelength was $\lambda \approx 10$ mm. The velocity field was measured on the liquid surface. It turned out that the energy spectrum $\mathcal{E}(k)$ of the horizontal motion had an inflection near the wave number $k_\mathrm{f} \approx 0.12$ mm^{-1} that approximately corresponded to the wavelength. In the region $k < k_\mathrm{f}$, the dependence was close to $\mathcal{E}(k) \propto k^{-5/3}$; in the region $k > k_\mathrm{f}$, the behavior $\mathcal{E}(k) \propto k^{-3}$ was observed (see expressions (B5) and (B6)), although the ranges of the corresponding power dependences were rather short, especially in the region $k > k_\mathrm{f}$. Additionally, mean energy and enstrophy fluxes were measured. They had signs corresponding to the picture of an inverse energy cascade in the region $k < k_\mathrm{f}$ and a direct enstrophy cascade at $k > k_\mathrm{f}$ characteristic of two-dimensional turbulence, although they were not constant in scale. Finally, studies of the relative dispersion of passive particles were in agreement with Richardson's law (B4).

Subsequent experiments were carried out on the surface of deep water in a wide range of parameters [22, 23]. Surprisingly, the surface flow still exhibited properties characteristic of a two-dimensional turbulent flow, although the depth of the liquid was greater than the wavelength. In the region of an inverse energy cascade, the spectrum of the horizontal flow $\mathcal{E}(k)$ showed a slope of $-5/3$, in accordance with expression (B5), and the direction of the energy flux was confirmed by measuring the triple correlator (B7). The region of a direct cascade $k > k_\mathrm{f}$ was short and was not studied in detail. The excitation of Faraday waves in a small square cell resulted in the formation of a large-scale coherent vortex. This is qualitatively similar to the condensation of energy in two-dimensional turbulence when the size of the system is less than the scale at which dissipation stops an inverse energy cascade (see [97–100]). Similar behavior was observed in a later experiment by another group [53], in which surface waves were excited by plungers, the depth of the liquid was ≈ 4 cm, and the wavelength was ≈ 5 cm. In the region $k < k_\mathrm{f}$, the energy spectrum of the vortex flow $\mathcal{E}(k) \propto k^{-5/3}$ was measured, and, at the largest scales, there was a peak corresponding to the directly observed statistically stable large-scale vortex.

The results contradict the expectation that large horizontal flows should penetrate deeper into the liquid than smaller flows, which, in turn, would violate the picture underlying the model of two-dimensional turbulence. Measurements of the dependence of the vortex flow on the distance to the surface were carried out in Refs [24, 25]. They showed that the velocity and kinetic energy of horizontal flows decreased sharply at distances of half a wavelength below the surface. Below this layer, the flow was three-dimensional, was considerably less intense, and had large correlation times and scales. The motion in the depth arose owing to jets that were formed on the surface and penetrated deep. The presence of such jets was identified by measuring the two-dimensional divergence of the velocity field on the surface and then confirmed by PIV measurements in a vertical slice.

Today, these experimental observations await a theoretical explanation. It remains unclear whether waves participate in the formation of large-scale vortices through the action of a virtual surface stress or a vortex force correlated with the vortex flow or their role is limited to the excitation of vortices with a horizontal size of the order of the wavelength. Estimates made on the basis of experimental data show that the vortex force integrated over height is significantly greater than the virtual wave stress (see expression (64)). Experiments [101, 102], in which a three-dimensional statistically stationary turbulent flow in the bulk under a free surface was excited by jets from the bottom, show that some not very pronounced elements of an inverse cascade are observed near the surface. Namely, the horizontal integral scale near the surface is ≈ 2 times greater than in the bulk, and the root-mean-square horizontal velocity near the surface is ≈ 1.5 times greater than in the bulk. Numerical calculations for attenuating turbulence demonstrate qualitatively similar results [103]. However, it can be assumed that, in this formulation of the problem, three-dimensional turbulent pulsations coming from the bulk to the free surface do not allow an inverse cascade to be formed near it.

6. Conclusions

Waves on the surface of water are often described within the potential approximation and the model of an ideal liquid. It is important to understand that this description has its limitations. The consideration of small but nonzero viscosity of the liquid leads not only to a decrease in the amplitude of surface waves in space or time but also to the generation of slow vortex flows that ensure the fulfillment of the momentum conservation law. The momentum is transferred from attenuating waves to a slow flow in a thin viscous sublayer near the surface, where the viscosity of the liquid violates the potential approximation. We emphasize that, in an ideal liquid, the excitation of vortex flows by potential waves is prohibited by Kelvin's theorem.

Slow currents are excited by a surface force (a virtual wave stress) and spread into the bulk of fluid due to viscous friction. In a steady-state regime, the amplitude of the slow flows significantly affects the Lagrangian velocity, which describes the motion of infinitesimal fluid elements. In addition to the slow flows, rapid wave motion also contributes to the Lagrangian velocity. The contribution from the waves is called the Stokes drift, and, as the analysis for the case of a free surface shows, it can be calculated within the model of an ideal liquid. The Stokes drift responds almost instantaneously to changes in the amplitude of surface waves.

In practice, the fluid surface is often contaminated, meaning it is covered by a thin adsorbed film. The presence of a film on the surface increases the dissipation of surface waves and consequently also enhances the generation of the slow flows. In this case, in the steady-state regime, the Lagrangian velocity is determined by the slow flow, and the Stokes drift can be disregarded.

An increase in the amplitude of the vortical flow leads to increased nonlinearity. The total flow in the volume can no longer be considered purely potential due to the presence of the slow vortical flow. The vorticity that slowly changes in

time gives rise to a weak vorticity oscillating together with the wave motion through nonlinear interaction. As a result, a volume vortex force arises, acting from the waves on the mean flow, and the waves themselves begin to scatter and refract on the slow vortical flow. In experiments where the vortical flow is generated solely by surface waves, an increase in the amplitude of the surface wave ensemble leads to the chaoticization of the slow flows, and their statistical properties largely resemble those of two-dimensional turbulent flow. A theoretical explanation for the experimental results in this regime remains an open question at present.

In the case of weak nonlinearity, the presented theory allows describing Lagrangian particle transport in the field of interfering waves. It has been demonstrated that the interference effects can enable the control of the transport of particles, bacteria, and active matter by tuning the wave field [20, 104]. By manipulating the distribution of particles on the surface of a fluid, one can potentially control its physical properties, which provides opportunities to create two-dimensional biocompatible materials with remotely tunable characteristics [14]. Furthermore, rapid wave and slow vortical flows act as external factors and influence bacterial life activities, allowing the cultivation of biofilms with tailored properties [105]. The results presented in this review may also find application in describing surface motion of the ocean and the propagation of plankton and pollutants near its surface [106].

Acknowledgments
This study was supported by the Ministry of Science and Higher Education of the Russian Federation (funding from FFWR-2024-0017 for S.S.V. and V.M.P. and FFWE-2025-0016 for A.A.L.) and by the Basic Research Program of HSE University.

7. Appendices

A. Viscous boundary layer on free surface

Here, we develop a mathematical framework for describing the viscous sublayer that moves and tilts with the fluid boundary. One version of such a framework was constructed in [2]. We aim to keep the mathematical complexity to a minimum, based on the premise that the description should be confined to the thickness of the viscous boundary layer and limited to the second order in wave amplitude. Let us introduce an auxiliary curvilinear coordinate system $\{t, x, y, \zeta\}$ with a new vertical coordinate $\zeta = z - h(t, x, y)$, in terms of which the boundary always has a flat form $\zeta = 0$. The description of the viscous sublayer is confined to values $\zeta \sim \delta$, so the specific nature of the coordinate transformation at depths of the order of the wavelength is not important to us. The rules for recalculating derivatives are

$$\partial_t = \widetilde{\partial}_t - \partial_t h \partial_\zeta\,, \quad \partial_\alpha = \widetilde{\partial}_\alpha - \partial_\alpha h \partial_\zeta\,, \quad \partial_z = \partial_\zeta\,. \tag{A1}$$

Here, differentiation in the curvilinear coordinate system is denoted by a tilde. The constructed curvilinear coordinates are not orthogonal, so we also need to introduce an orthogonal matrix $\mathcal{O}_{ij} = \delta_{ij} + \delta_{iz}\partial_j h - \partial_i h \delta_{jz}$, which rotates the local orthogonal coordinate system so that the third axis is directed along the normal to the fluid surface, $l_i = \mathcal{O}_{iz}$. The components of velocity and vorticity in the new coordinates $\widetilde{\varpi}_i$ are related to the components of vorticity ϖ_i in the original Cartesian coordinates by relations like $\varpi_i = \mathcal{O}_{ij}\widetilde{\varpi}_j$. Note that we define the transformations with an accuracy up to the first order in wave amplitude h, since, in the Navier–Stokes equation, we need to account for no more than the second order in h. With this accuracy, the vorticity equation (37) in the new coordinates takes the form

$$\widetilde{\partial}_t \widetilde{\boldsymbol{\varpi}} = -\big((\widetilde{\mathbf{v}} - \mathbf{e}^z \partial_t h)\widetilde{\nabla}\big)\widetilde{\boldsymbol{\varpi}} + \big(\widetilde{\boldsymbol{\varpi}}\widetilde{\nabla}\big)(\widetilde{\mathbf{v}} - \mathbf{e}^z \partial_t h) + \widetilde{\varpi}_\zeta \widetilde{\nabla}\partial_t h + \nu \partial_\zeta^2 \widetilde{\boldsymbol{\varpi}}\,, \tag{A2}$$

where $\mathbf{e}^z$ is the unit vector directed upward, and in the last term, corrections of order γ^2 have been neglected. The correction in the first term on the right-hand side of (A2) accounts for the fact that the advection of vorticity by the flow, leading to a change in its distribution relative to the fluid surface, must be measured relative to that surface. The corrections in the second and the third terms account for the subtraction of the rotation occurring together with the rotation of the surface. Since we perform calculations with an accuracy only up to quadratic contributions in the wave amplitude, in the nonlinear contributions in (A2), there is no need to account for the difference between the vectors $\boldsymbol{\varpi}^u$ and $\widetilde{\boldsymbol{\varpi}}^u$. In the linear approximation in the wave amplitude, equation (30) takes the form $\widetilde{\partial}_t \widetilde{\varpi}_\alpha^u = \nu \partial_\zeta^2 \widetilde{\varpi}_\alpha^u$ with boundary conditions

$$\nu \widetilde{\varpi}_\alpha^u\big|_{\zeta=0} = \epsilon_{\alpha\beta}\partial_\alpha(\sigma' n - 2\nu \partial_z \phi)\big|_{z=0}\,, \quad \partial_\zeta \widetilde{\varpi}_\zeta^u\big|_{\zeta=0} = 0\,, \tag{A3}$$

following from (34), (38). On the right-hand side, the value of the potential part of the velocity is sufficient to compute on the unperturbed surface $z = 0$, since condition (1) holds for any surface shape, so the exponential dependence on the vertical coordinate is determined by the periodic dependence in the horizontal direction. The boundary condition in the form (A3) was discussed, in particular, in [80, 107].

B. Interaction between surface waves and slow vortex flow

The Navier–Stokes equation (30), averaged over rapid wave oscillations, can be written as

$$\partial_t \mathbf{V} + (\mathbf{V}\nabla)\mathbf{V} = -\nabla\left\langle \frac{P}{\rho} + \frac{u^2}{2}\right\rangle + \nu\Delta\mathbf{V} + \big\langle[\mathbf{u}, \boldsymbol{\varpi}^u]\big\rangle\,. \tag{B1}$$

Using (62), it is possible to rewrite the last term in (B1) in a more convenient form,

$$\big\langle[\mathbf{u}^\phi \times \boldsymbol{\varpi}^u]\big\rangle = \mathbf{f}^{\mathrm{V}} + \operatorname{grad}(\boldsymbol{\Omega}\boldsymbol{\mathcal{A}})\,, \quad \mathbf{f}^{\mathrm{V}} = [\mathbf{U}^{\mathrm{S}} \times \boldsymbol{\Omega}]\,, \tag{B2}$$

where the vector $\boldsymbol{\mathcal{A}} = \langle[\operatorname{grad}\phi \times \delta\mathbf{R}_1]\rangle/2$. In performing the derivations, we used the fact that the potential flow is incompressible, so, in particular, $\operatorname{div}\delta\mathbf{R}_1 = 0$; moreover, $\langle u_i\,\delta R_{1j}\rangle = -\langle u_j\,\delta R_{1i}\rangle$. The Stokes drift previously defined in (27) is

$$\mathbf{U}^{\mathrm{S}} = \operatorname{rot}\boldsymbol{\mathcal{A}} = \big\langle \operatorname{rot}[\mathbf{u}^\phi \times \delta\mathbf{R}_1]\big\rangle\,; \tag{B3}$$

it is determined solely by the potential part of the wave flow in the fluid bulk. The gradient contribution in (B2) should be included in the effective pressure in (B1), so the effective pressure in (63) is

$$\frac{\overline{\mathcal{P}}}{\rho} = \frac{\mathcal{P}}{\rho} + \frac{\mathbf{V}^2 + \langle\mathbf{u}^2\rangle}{2} - (\boldsymbol{\Omega}\boldsymbol{\mathcal{A}})\,. \tag{B4}$$

Note that all time averages $\langle \ldots \rangle$ in (B1)–(B3) must be performed along the Lagrangian trajectories $\mathbf{r}(t)$ defined after (62).

Let us now proceed to the short-wave limit (see Section 4.4). We will first describe how to extract the imaginary part on the right-hand side of the wave equation (76) multiplied by $\exp(-\mathrm{i}\varphi)$. Consider a neighborhood of some point '0', where we place the origin of coordinates. The phase can be expanded in a Taylor series

$$\varphi = \varphi^0 + k_i^0 r_i + \frac{1}{2}\,(\partial_j k_i)^0 r_i r_j + \ldots . \tag{B5}$$

On the right-hand side of (76), the quantity $\omega_{\hat{k}}^2$ should be considered an integro-differential operator. Let us expand this operator near the carrier wave vector $\mathbf{k}^0 = \operatorname{grad}\varphi|_{\mathbf{r}=0}$:

$$-\omega^2_{\mathbf{k}^0 - \mathrm{i}\nabla} \approx -\omega^2_{\mathbf{k}^0} + 2\mathrm{i}\omega_{\mathbf{k}^0} v_i^{\mathrm{g}0}\partial_i + \frac{\partial\left(\omega_{\mathbf{k}^0} v_i^{\mathrm{g}0}\right)}{\partial k_j^0}\,\partial_j\partial_i + \ldots . \tag{B6}$$

As a result, the imaginary part (we omit the '0' indices) is

$$\begin{aligned} &-\operatorname{Im}\left(\exp(-\mathrm{i}\varphi)\omega_{\hat{k}}^2\left(|\psi|\exp(\mathrm{i}\varphi)\right)\right) \\ &\quad = 2\omega_k(\mathbf{v}^{\mathrm{g}}\nabla)|\psi| + |\psi|\operatorname{div}\left(\omega_k\,\mathbf{v}^{\mathrm{g}}\right). \end{aligned} \tag{B7}$$

Now let us perform the calculations for the left-hand side of equation (76), starting with the formal calculation

$$\begin{aligned} &\varepsilon_{\hat{k}}\,\hat{\tilde{\omega}}\,\frac{1}{\varepsilon_{\hat{k}}}\,\hat{\tilde{\omega}}'\left(|\psi|\exp(\mathrm{i}\varphi)\right) \\ &\quad = \hat{\tilde{\omega}}\,\hat{\tilde{\omega}}'\left(|\psi|\exp(\mathrm{i}\varphi)\right) + \varepsilon_{\hat{k}}\left(\hat{\tilde{\omega}}\,\frac{1}{\varepsilon_{\hat{k}}} - \frac{1}{\varepsilon_{\hat{k}}}\,\hat{\tilde{\omega}}\right)\hat{\tilde{\omega}}'\left(|\psi|\exp(\mathrm{i}\varphi)\right), \end{aligned} \tag{B8}$$

where the operators are $\hat{\tilde{\omega}} = \mathrm{i}(\partial_t + V_\alpha\partial_\alpha)$, $\hat{\tilde{\omega}}' = \mathrm{i}(\partial_t + \partial_\alpha V_\alpha)$. The second term on the right-hand side of (B8) is determined by the nonzero value of the commutator in parentheses:

$$\begin{aligned} &\left(\hat{\tilde{\omega}}\,\frac{1}{\varepsilon_{\hat{k}}} - \frac{1}{\varepsilon_{\hat{k}}}\,\hat{\tilde{\omega}}\right)\exp(\mathrm{i}\varphi) \\ &\quad = \exp(\mathrm{i}\varphi)\left(\hat{\tilde{\omega}}\,\frac{1}{\varepsilon_k} - \frac{1}{\varepsilon_k^2}\,\frac{\mathrm{d}\varepsilon_k}{\mathrm{d}\omega_k}\,\frac{\partial\omega_k}{\partial k_\alpha}\,\frac{\partial\omega_k}{\partial r_\alpha}\right) \\ &\quad = \exp(\mathrm{i}\varphi)\left(\partial_t + \left((\mathbf{V} + \mathbf{v}^{\mathrm{g}})\nabla\right)\right)\frac{1}{\varepsilon_k}\,. \end{aligned} \tag{B9}$$

The first term on the right-hand side of (B8) is calculated relatively straightforwardly up to the first derivatives of the slowly varying quantities. After extracting the imaginary parts, both sides of equation (76) must also be multiplied by $|\psi|/\varepsilon_k$ to obtain equation (80).

Finally, note that the wave equation (76) can be regarded as a consequence of the requirement that the variation in the action

$$S = \int \mathrm{d}t\,\mathrm{d}x\,\mathrm{d}y\left(\left((\partial_t + \partial_\beta V_\beta)\psi\right)\frac{1}{\varepsilon_{\hat{k}}}\left((\partial_t + \partial_\alpha V_\alpha)\psi\right) - \psi\hat{k}\psi\right) \tag{B10}$$

be zero on the true trajectory. The condition that the variation in the action (B10) with respect to the phase φ of the potential ψ be zero leads to the conservation law for the wave action (80) (see, for example, [84, § 11.7] or [85, § 4.11]).

C. Two-dimensional turbulence

The motion of a two-dimensional turbulent flow can be described by the modified Navier–Stokes equation

$$\partial_t\mathbf{v} + (\mathbf{v}\nabla)\mathbf{v} = -\frac{\nabla p}{\rho} + \nu\nabla^2\mathbf{v} - \alpha\mathbf{v} + \mathbf{f}. \tag{C1}$$

Here, the velocity field $\mathbf{v}$ is two-dimensional and incompressible, $\partial_\alpha v_\alpha = 0$. Compared to Eqn (30), the right side is supplemented by an external force $\mathbf{f}$, which excites the flow, and by a dissipative term $-\alpha\mathbf{v}$, which describes the linear friction against the bottom. Physically, this equation describes the motion of a thin layer of the liquid on scales greater than its thickness, and the friction against the bottom is related to the three-dimensionality of the problem. Hereafter, we will assume that the external force $\mathbf{f}$ has a characteristic scale $l_{\mathrm{f}} \sim 1/k_{\mathrm{f}}$ and a power $\epsilon = \langle\mathbf{v}\,\mathbf{f}\rangle$, where the angle brackets denote averaging over space and time.

Along with the velocity $\mathbf{v}$, the motion of the liquid can be characterized by vorticity, which is a pseudoscalar $\varpi = \partial_x v_y - \partial_y v_x$ in the two-dimensional case. The equation for vorticity follows from the Navier–Stokes equation (C1)

$$\partial_t\varpi + \mathbf{v}\nabla\varpi = \nu\nabla^2\varpi - \alpha\varpi + f_\varpi\,, \tag{C2}$$

where $f_\varpi = \partial_x f_y - \partial_y f_x$. In the absence of dissipation and pumping, Eqns (C1) and (C2) conserve not only the energy of the system $E = (1/S)\int \mathrm{d}x\,\mathrm{d}y\,\mathbf{v}^2/2$ but also its enstrophy $Z = (1/S)\int \mathrm{d}x\,\mathrm{d}y\,\varpi^2/2$, where S is the area of the system. The presence of an additional quadratic integral of motion fundamentally distinguishes the behavior of a two-dimensional turbulent system from that of its three-dimensional analogue.

At a qualitative level, the following occurs. An external force pumps the energy ϵ and enstrophy $\eta = \langle\varpi f_\varpi\rangle \sim \epsilon k_{\mathrm{f}}^2$ into the system per unit time. For a turbulent flow, dissipation on the pumping scale is negligible; hence, these conserved quantities begin to redistribute over scales due to nonlinear interactions. It turns out that the enstrophy flux is directed toward small scales and forms the so-called direct enstrophy cascade. Assuming that the typical velocity fluctuations δv on the scale r in the direct cascade depend only on the enstrophy flux η and the scale r, one can obtain the estimate $\delta v \sim \eta^{1/3} r$, where $r \ll l_{\mathrm{f}}$ from dimensional considerations. Next, by using this estimate for the velocity fluctuations and comparing the nonlinear and viscous terms in the Navier–Stokes equation with each other, it can be established that the viscosity of the liquid will come into play and stop the direct cascade on the scale $L_{\mathrm{d}} \sim \nu^{1/2}\eta^{-1/6}$.

The energy flux is directed in the opposite direction and results in the excitation of increasingly larger-scale flows. If we similarly assume that the typical fluctuations in the velocity on the scale r in the inverse energy cascade depend only on the energy flux ϵ and the scale r, we can obtain the estimate $\delta v \sim (\epsilon r)^{1/3}$, where $r \gg l_{\mathrm{f}}$. The inverse cascade is stopped by friction against the bottom, and this occurs on the scale

$$L_\alpha \sim \epsilon^{1/2}\alpha^{-3/2}\,, \tag{C3}$$

when this mechanism is able to dissipate all the power ϵ pumped in by the external force. The regime of developed turbulence assumes the fulfillment of inequalities $L_{\mathrm{d}} \ll l_{\mathrm{f}} \ll L_\alpha$, which means that dissipation on the pumping

scale due to the viscosity and friction against the bottom is small compared to nonlinearity [108].

In the region of the inverse energy cascade $l_f \ll r \ll L_\alpha$, one of the consequences of the estimate of velocity fluctuations $\delta v \sim (\epsilon r)^{1/3}$ is Richardson's law, which describes particles passively carried by a flow moving apart from each other. Let us consider two particles separated by the distance R. Over time, this distance will increase, and the main contribution to this process will be made by fluctuations with a scale of R, i.e., $\mathrm{d}R/\mathrm{d}t \sim (\epsilon R)^{1/3}$. Larger fluctuations will carry both particles in the same way, while smaller fluctuations will do that considerably more weakly. In experiments, the root-mean-square distance between particles is usually measured, for which the following solution is obtained:

$$\langle R^2 \rangle \sim \epsilon t^3 . \tag{C4}$$

Here, averaging is implied over pairs of particles that were at the same distance from each other at the initial moment of time. On average, the particles move apart faster than at the diffusion behavior $\langle R^2 \rangle \propto t$ and faster than under ballistic motion $\langle R^2 \rangle \propto t^2$.

Turbulent motion is traditionally characterized by an energy spectrum that describes the distribution of energy over scales. By using Parseval's theorem, the energy of the system can be presented as the sum of Fourier harmonics for the velocity field $E = \sum_{\mathbf{k}} |\hat{\mathbf{v}}_{\mathbf{k}}|^2/2$, where $\hat{\mathbf{v}}_{\mathbf{k}} = (1/S) \int \mathrm{d}x\, \mathrm{d}y\, \mathbf{v}(\mathbf{r}) \exp(\mathrm{i}\mathbf{k}\mathbf{r})$. The expression under the summation sign is called the two-dimensional energy spectrum. In practice, one usually works with a one-dimensional energy spectrum $\mathcal{E}(k)$, which is obtained from a two-dimensional one by averaging over the angle, i.e., $\mathcal{E}(k) = \pi k \langle |\hat{\mathbf{v}}_{\mathbf{k}}|^2 \rangle$, where the angle brackets mean averaging over all $|\mathbf{k}| = k$. According to this definition, the energy and enstrophy of the system are $E = \int \mathrm{d}k\, \mathcal{E}(k)$ and $Z = \int \mathrm{d}k\, k^2 \mathcal{E}(k)$. Previous estimates for fluctuations of the velocity in the regions of the inverse and direct cascades allow us to obtain the following expressions for the one-dimensional energy spectrum [55]:

$$\mathcal{E}(k) \sim \epsilon^{2/3} k^{-5/3}, \qquad \frac{1}{L_\alpha} \ll k \ll k_f, \tag{C5}$$

$$\mathcal{E}(k) \sim \eta^{2/3} k^{-3}, \qquad k_f \ll k \ll \frac{1}{L_d} . \tag{C6}$$

These dependences are shown schematically in Fig. 5.

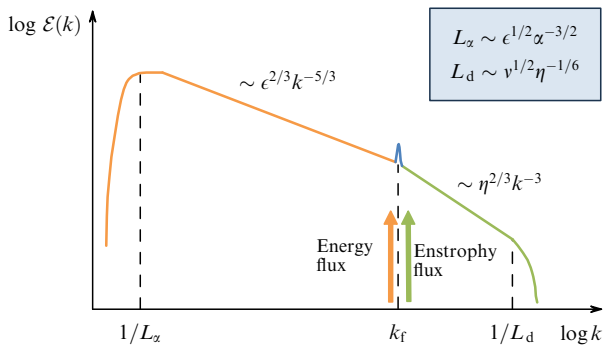

Figure 5. Schematic of energy spectrum of two-dimensional turbulent flow.

An analysis of the Navier–Stokes equation (C1) allows us to establish an exact relation for the third-order correlation function $S_3(r) = \langle (\mathbf{v}_1 - \mathbf{v}_2)_r^3 \rangle$, which is an analogue of the Kolmogorov relation for developed three-dimensional turbulence. Here, indices 1 and 2 denote the quantities taken at points $\mathbf{r}_1$ and $\mathbf{r}_2$, and $(\mathbf{v}_1 - \mathbf{v}_2)_r$ denotes the projection of the difference of velocities onto the vector $\mathbf{r} = \mathbf{r}_1 - \mathbf{r}_2$ and $r = |\mathbf{r}|$. In the regions of the inverse and direct cascades, the relations take the form [55]

$$S_3(r) = \frac{3}{2} \epsilon r, \qquad l_f \ll r \ll L_\alpha , \tag{C7}$$

$$S_3(r) = \frac{1}{8} \eta r^3 , \qquad L_d \ll r \ll l_f \tag{C8}$$

and express the constancy of the energy and enstrophy fluxes over the scales, respectively. In the case of three-dimensional turbulence, the Kolmogorov relation has a different sign, $S_3(r) = -4\epsilon r/5$, compared to expression (C7), reflecting the opposite direction of the energy flux. In three-dimensional turbulent systems, energy is transferred from the pumping scale to small scales, and enstrophy is not a conserved quantity; therefore, its cascade does not exist.

For the sake of completeness, we shall briefly discuss characteristic times of the formation of cascades. After switching on pumping, a direct enstrophy cascade is formed very quickly, in a period of time that can be estimated as $\eta^{-1/3}$. An inverse energy cascade is formed considerably more slowly, since it involves the excitation of motions with increasingly larger scales $l(t)$. During time t, only motions with a characteristic time $l/\delta v \lesssim t$ can be excited, from which we find the estimate $l(t) \sim \epsilon^{1/2} t^{3/2}$. The formation of the inverse cascade finishes when $l(t)$ reaches the scale L_α.

So far, we have assumed that the size of the two-dimensional system under consideration is greater than L_α. If the size of the system is $L < L_\alpha$, the inverse energy cascade will have to stop at the scale L. Since the friction against the bottom α cannot completely dissipate the energy ϵ supplied by pumping at this scale, it will accumulate (in other words, condense) at the scale L. As a result, a large-scale coherent flow will arise in the system, which is able to change significantly the energy spectrum of the system and modify the inverse cascade. The structure of the coherent flow depends strongly on the boundary conditions. For a square cell with non-slip boundaries, the formation of a large-scale coherent vortex was observed in laboratory and numerical experiments [97–100, 109].

References

1. Stokes G G *Trans. Cambridge Philos. Soc.* **8** 441 (1847)
2. Longuet-Higgins M S *Philos. Trans. R. Soc. A* **245** 535 (1953) DOI:10.1098/rsta.1953.0006
3. Longuet-Higgins M S *Proc. R. Soc. London A* **311** 371 (1969)
4. Weber J E *J. Geophys. Res. Oceans* **106** 11653 (2001)
5. Stuart J T *J. Fluid Mech.* **24** 673 (1966)
6. Ünlüata U, Mei C C *J. Geophys. Res.* **75** 7611 (1970)
7. Dore B D *Quart. J. Mech. Appl. Math.* **30** 157 (1977)
8. Madsen O S *J. Phys. Oceanogr.* **8** 1009 (1978)
9. Weber J E *J. Fluid Mech.* **137** 115 (1983)
10. Xu Z, Bowen A J *J. Phys. Oceanogr.* **24** 1850 (1994)
11. Eeltink D et al. *Wave Motion* **97** 102610 (2020)
12. Filatov S V et al. *Phys. Rev. Lett.* **116** 054501 (2016)
13. Filatov S V, Aliev S A, Levchenko A A, Khramov D A *JETP Lett.* **104** 702 (2016); *Pis'ma Zh. Eksp. Teor. Fiz.* **104** 714 (2016)
14. Francois N et al. *Nature Commun.* **8** 14325 (2017)

15. Xia H et al. *Fluids* **4** (2) 74 (2019)
16. Abella A P, Soriano M N *Phys. Scr.* **95** 085007 (2020)
17. Filatov S V, Orlov A V, Brazhnikov M Yu, Levchenko A A *JETP Lett.* **108** 519 (2018); *Pis'ma Zh. Eksp. Teor. Fiz.* **108** 549 (2018)
18. Abella A P, Soriano M N *J. Exp. Theor. Phys.* **130** 452 (2020); *Zh. Eksp. Teor. Fiz.* **157** 539 (2020)
19. Smirnova D A, Nori F, Bliokh K Y *Phys. Rev. Lett.* **132** 054003 (2024)
20. Wang B et al. *Nature* **638** 394 (2025)
21. von Kameke A et al. *Phys. Rev. Lett.* **107** 074502 (2011)
22. Francois N et al. *Phys. Rev. Lett.* **110** 194501 (2013)
23. Francois N et al. *Phys. Rev. X* **4** 021021 (2014) DOI:10.1103/PhysRevX.4.021021
24. Colombi R, Schlüter M, von Kameke A *Exp. Fluids* **62** 8 (2021)
25. Colombi R et al. *Fluids* **7** (5) 148 (2022)
26. Levich V G *Zh. Eksp. Teor. Fiz.* **10** 1296 (1940)
27. Levich V G *Zh. Eksp. Teor. Fiz.* **11** 340 (1941)
28. Levich V G *Physicochemical Hydrodynamics* (Englewood Cliffs, NJ: Prentice-Hall, 1962) translated from Russian 1st ed.; 3rd Russian ed., rev. and enlarged *Fiziko-khimicheskaya Gidrodinamika* (Moscow–Izhevsk: Inst. Komp'yut. Issled., 2016)
29. Miles J W *Proc. R. Soc. London A* **297** 459 (1967)
30. Lucassen-Reynders E H, Lucassen J *Adv. Colloid Interface Sci.* **2** 347 (1970)
31. Henderson D M *J. Fluid Mech.* **365** 89 (1998)
32. Henderson D M, Segur H *J. Geophys. Res. Oceans* **118** 5074 (2013)
33. Campagne A et al. *Phys. Rev. Fluids* **3** 044801 (2018)
34. Van Dorn W G *J. Fluid Mech.* **24** 769 (1966)
35. Parfenyev V M, Vergeles S S, Lebedev V V *Phys. Rev. E* **94** 052801 (2016)
36. Parfenyev V M, Vergeles S S *Phys. Rev. Fluids* **3** 064702 (2018)
37. Parfenyev V M et al. *Phys. Rev. Fluids* **4** 114701 (2019)
38. Langevin D *Annu. Rev. Fluid Mech.* **46** 47 (2014)
39. Francois N et al. *Phys. Rev. E* **92** 023027 (2015)
40. Parfenyev V M, Vergeles S S *Phys. Rev. Fluids* **5** 094702 (2020)
41. Filatov S V, Poplevin A V, Levchenko A A, Parfenyev V M *Physica D* **434** 133218 (2022)
42. Riley N *Annu. Rev. Fluid Mech.* **33** 43 (2001)
43. Lord Rayleigh *Philos. Trans. R. Soc. London* **175** 1 (1884)
44. Boluriaan S, Morris P *Int. J. Aeroacoust.* **2** 255 (2003)
45. Landau L D, Lifshitz E M *Fluid Mechanics* (Oxford: Pergamon Press, 1987); Translated from Russian: *Gidrodinamika* (Moscow: Fizmatlit, 2001)
46. Subbotin S, Shiryaeva M *Microgravity Sci. Technol.* **34** 89 (2022)
47. Subbotin S et al. *Phys. Fluids* **35** 074110 (2023)
48. Riley N *IMA J. Appl. Math.* **3** 419 (1967) DOI:10.1093/imamat/3.4.419
49. Lyubimova T P et al. *Microgravity Sci. Technol.* **37** 45 (2025)
50. Parfenyev V M, Vergeles S S, Lebedev V V *JETP Lett.* **103** 201 (2016); *Pis'ma Zh. Eksp. Teor. Fiz.* **103** 220 (2016)
51. Parfenyev V M, Vergeles S S, Lebedev V V *JETP Lett.* **104** 287 (2016)
52. Yablonskii S V, Kurbatov N M, Parfenyev V M *Phys. Rev. E* **95** 012707 (2017)
53. Filatov S V, Levchenko A A, Mezhov-Deglin L P *JETP Lett.* **111** 549 (2020); *Pis'ma Zh. Eksp. Teor. Fiz.* **111** 653 (2020)
54. Filatov S V, Khramov D A, Levchenko A A *JETP Lett.* **106** 330 (2017); *Pis'ma Zh. Eksp. Teor. Fiz.* **106** 305 (2017)
55. Boffetta G, Ecke R E *Annu. Rev. Fluid Mech.* **44** 427 (2012)
56. Craik A D D, Leibovich S *J. Fluid Mech.* **73** 401 (1976)
57. Holm D D *Physica D* **98** 415 (1996)
58. Vergeles S S, Vointsev I A *Phys. Fluids* **36** 034119 (2024); arXiv:2310.19533
59. Abrashkin A A, Pelinovsky E N *Phys. Usp.* **65** 453 (2022); *Usp. Fiz. Nauk* **192** 491 (2022)
60. Stewart R H, Joy J W *Deep Sea Res. Oceanogr. Abstracts* **21** 1039 (1974)
61. Andrews D G, McIntyre M *J. Fluid Mech.* **89** 647 (1978)
62. Fabrikant A L, Stepanyants Yu A *Propagation of Waves in Shear Flows* (Singapore: World Scientific, 1998); Translated from Russian: *Rasprostranenie Voln v Sdvigovykh Potokakh* (Moscow: Fizmatlit, 1996)
63. Peregrine D H *Adv. Appl. Mech.* **16** 9 (1976)
64. Basovich A Ya, Talanov V I *Izv. Akad. Nauk SSSR. Fiz. Atmos. Okeana* **13** 766 (1977)
65. Craik A D D *J. Fluid Mech.* **81** 209 (1977)
66. Lamb H *Hydrodynamics* 6th ed. (Cambridge: Cambridge Univ. Press, 1975)
67. Longuet-Higgins M S, Stewart R W *J. Fluid Mech.* **8** 565 (1960)
68. Longuet-Higgins M S, Stewart R *Deep Sea Res. Oceanogr. Abstracts* **11** 529 (1964)
69. van den Bremer T S, Breivik Ø *Philos. Trans. R. Soc. A* **376** 20170104 (2018)
70. Monismith S G *J. Fluid Mech.* **884** F1 (2020)
71. van den Bremer T S et al. *J. Fluid Mech.* **879** 168 (2019)
72. Calvert R et al. *Phys. Rev. Fluids* **4** 114801 (2019)
73. Phillips O M *The Dynamics of the Upper Ocean* (Cambridge: Cambridge Univ. Press, 1977); Translated into Russian: *Dinamika Verkhnego Sloya Okeana* (Leningrad: Gidrometeoizdat, 1980)
74. Stepanyants Yu A, Fabrikant A L *Sov. Phys. Usp.* **32** 783 (1989); *Usp. Fiz. Nauk* **159** 83 (1989)
75. Dysthe K B *Proc. R. Soc. London A* **369** 105 (1979)
76. Longuet-Higgins M S *J. Fluid Mech.* **17** 459 (1963)
77. Lucassen J *Trans. Faraday Soc.* **64** 2221 (1968)
78. Rajan G K *Int. J. Eng. Sci.* **154** 103340 (2020)
79. Alpers W, Hühnerfuss H *J. Geophys. Res. Oceans* **94** 6251 (1989)
80. Ruvinsky K D, Feldstein F I, Freidman G I *J. Fluid Mech.* **230** 339 (1991)
81. Gershuni G Z, Lyubimov D V *Thermal Vibrational Convection* (Chichester: John Wiley and Sons, 1998)
82. Belonozhko D F, Kozin A V *Fluid Dyn.* **46** 270 (2011)
83. Shmyrov A V et al. *J. Fluid Mech.* **877** 495 (2019)
84. Whitham G B *Linear and Nonlinear Waves* (New York: Wiley, 1974); Translated into Russian: *Lineinye i Nelineinye Volny* (Moscow: Mir, 1977)
85. Kamchatnov A M *Teoriya Lineinykh i Nelineinykh Voln* (Theory of Linear and Nonlinear Waves) (Moscow: Izd. Dom Vysshei Shkoly Ekonomiki, 2025)
86. Lee K, Mizutani N *Int. J. Offshore Polar Eng.* **17** 259 (2007)
87. Romero L, Lenain L, Melville W K *J. Phys. Oceanogr.* **47** 615 (2017)
88. Thorpe S A *Annu. Rev. Fluid Mech.* **36** 55 (2004)
89. Fox-Kemper B, Johnson L, Qiao F, in *Ocean Mixing: Drivers, Mechanisms and Impacts* (Eds M Meredith, A N Garabato) (Amsterdam: Elsevier, 2022) pp. 65–94, DOI:10.1016/B978-0-12-821512-8.00011-6
90. Samodurov A S et al. *Phys. Oceanogr.* **30** 689 (2023); Translated from Russian: *Morskoi Gidrofiz. Zh.* **39** 735 (2023)
91. Leibovich S *Annu. Rev. Fluid Mech.* **15** 391 (1983)
92. Kawamura T *J. Marine Sci. Technol.* **5** 161 (2000)
93. Fujiwara Y, Yoshikawa Y *J. Phys. Oceanogr.* **50** 2323 (2020)
94. Veron F, Melville W K *J. Fluid Mech.* **446** 25 (2001)
95. Craik A D D *J. Fluid Mech.* **125** 37 (1982)
96. Leibovich S *J. Fluid Mech.* **79** 715 (1977)
97. Molenaar D, Clercx H J H, van Heijst G J F *Physica D* **196** 329 (2004)
98. Xia H, Shats M, Falkovich G *Phys. Fluids* **21** 125101 (2009)
99. Bardóczi L et al. *Phys. Rev. E* **90** 063103 (2014)
100. Doludenko A N et al. *Phys. Fluids* **33** 011704 (2021)
101. Ruth D J, Coletti F *J. Fluid Mech.* **1001** A46 (2024)
102. Jamin T, Berhanu M, Falcon E *Phys. Rev. Fluids* **10** 034608 (2025); arXiv:2401.17871
103. Flores O, Riley J J, Horner-Devine A R *J. Fluid Mech.* **821** 248 (2017)
104. Gorce J-B et al. *Proc. Natl. Acad. Sci. USA* **116** 25424 (2019)
105. Hong S-H et al. *Sci. Adv.* **6** eaaz9386 (2020)
106. Falkovich G *J. Fluid Mech.* **638** 1 (2009)
107. Dias F, Dyachenko A I, Zakharov V E *Phys. Lett. A* **372** 1297 (2008)
108. Kolokolov I V, Lebedev V V, Parfenyev V M *Phys. Rev. E* **109** 035103 (2024)
109. Shikanian A, Parfenyev V *Phys. Fluids* **37** 095127 (2025)